



Review

Review of Piezoelectric Micromachined Ultrasonic Transducers for Rangefinders

Jiong Pan ¹, Chenyu Bai ¹, Qincheng Zheng ¹ and Huikai Xie ^{1,2,*} ¹ School of Integrated Circuits and Electronics, Beijing Institute of Technology (BIT), Beijing 100081, China² BIT Chongqing Center for Microelectronics and Microsystems, Chongqing 400030, China

* Correspondence: hk.xie@ieee.org

Abstract: Piezoelectric micromachined ultrasonic transducer (pMUT) rangefinders have been rapidly developed in the last decade. With high output pressure to enable long-range detection and low power consumption (16 μ W for over 1 m range detection has been reported), pMUT rangefinders have drawn extensive attention to mobile range-finding. pMUT rangefinders with different strategies to enhance range-finding performance have been developed, including the utilization of pMUT arrays, advanced device structures, and novel piezoelectric materials, and the improvements of range-finding methods. This work briefly introduces the working principle of pMUT rangefinders and then provides an extensive overview of recent advancements that improve the performance of pMUT rangefinders, including advanced pMUT devices and range-finding methods used in pMUT rangefinder systems. Finally, several derivative systems of pMUT rangefinders enabling pMUT rangefinders for broader applications are presented.

Keywords: pMUT; piezoelectric; rangefinder; range-finding; microelectromechanical system; MEMS

1. Introduction



Citation: Pan, J.; Bai, C.; Zheng, Q.; Xie, H. Review of Piezoelectric Micromachined Ultrasonic Transducers for Rangefinders. *Micromachines* **2023**, *14*, 374. <https://doi.org/10.3390/mi14020374>

Academic Editor: Wei Li

Received: 30 December 2022

Revised: 21 January 2023

Accepted: 30 January 2023

Published: 2 February 2023



Copyright: © 2023 by the authors. Licensee MDPI, Basel, Switzerland. This article is an open access article distributed under the terms and conditions of the Creative Commons Attribution (CC BY) license (<https://creativecommons.org/licenses/by/4.0/>).

Piezoelectric micromachined ultrasonic transducers, or pMUTs, are microelectromechanical system (MEMS) devices that convert electrical energy to mechanical energy or vice versa through the flexural vibration (or deflection) of a membrane composed of a thin piezoelectric film based on piezoelectric effects [1–3]. A system with a single or several pMUTs can be used to transmit [4], to receive [5], or to both transmit and receive ultrasound signals (e.g., a pMUT imager [6,7], flowmeter [8], or rangefinder [9,10]), as illustrated in Figure 1. This article is focused on pMUT rangefinders. A pMUT rangefinder takes advantage of the signal transmitting and receiving capability of pMUTs to obtain a range between the target and the device [11], containing a single pMUT, multiple pMUTs, or an array of pMUTs to perform both ultrasonic transmitting and receiving. A pMUT rangefinder is only responsible for finding the range of a target but not the angle and direction of the target; derivative systems made of groups of pMUT rangefinders are able to perform more complicated tasks such as target positioning and object detection based on a group of range data [12,13]. It should be noted that pMUT rangefinder systems are different from pMUT imaging systems in that the objectives of pMUT imaging systems are to acquire the spatial distribution or three-dimensional (3D) structural information of a target but not the distances between the pMUT and the target points [14].

pMUT rangefinders are promising in the relatively short-range (<10 m) detection for mobile use. Similar to other ultrasonic rangefinders, pMUT rangefinders are competitive to optical (light-based) rangefinder systems in relatively short-range detection because the speed of sound is much smaller than that of light, and they do not require high-speed electronic devices and their power consumptions are typically much lower. For instance, the power consumption of an optical rangefinder is greater than 1 W [13], while that of a pMUT rangefinder system can be only a few μ W. It has been reported that a pMUT

rangefinder can detect over a 1 m range under 16 μW of power consumption [15]. In addition, optical rangefinder systems are easily interfered with by sunlight or surrounding artificial lights, which may heavily affect range accuracy, limiting their use [16].

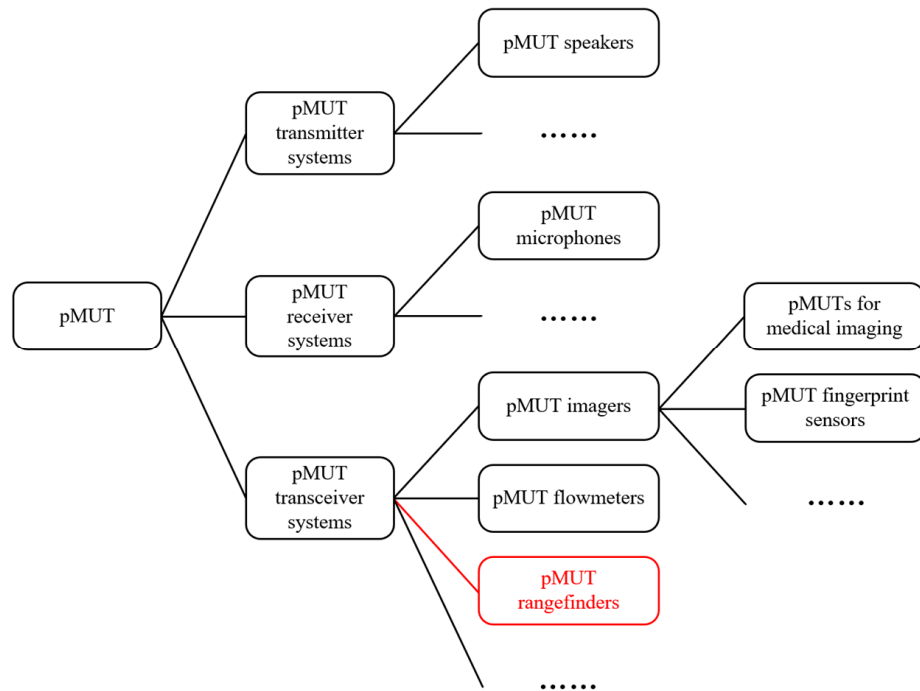


Figure 1. Different applications of pMUTs.

Secondly, compared to other ultrasonic rangefinders, pMUT rangefinders have their advantages. Currently, most commercially available ultrasonic rangefinders are made of bulk piezoelectric ultrasonic transducers due to their high output power [17], but they suffer from a series of drawbacks, including poor acoustic impedance matching [18] and large size [19]. Although incorporating acoustic matching layers can improve impedance matching [20], the bandwidth is limited, and it may not be practical in specific cases [21,22]. In contrast, pMUTs can have miniaturized size [23,24] and better acoustic matching [22,25], so a higher transmitting efficiency can be achieved. Furthermore, the small size of pMUTs not only enables pMUT rangefinders to be integrated with electronics, which saves space and energy for mobile use but also enables the fabrication of large ultrasonic transducer arrays, helping to realize more complicated systems [26–28]. Compared to ultrasonic rangefinders based on capacitive micromachined ultrasonic transducers (cMUTs) [29,30], pMUT rangefinders have a larger ultrasound output, lower bias voltage, and larger detectable range [31,32]. Hence, the low power consumption, relatively high output pressure, and integrated property of pMUT rangefinders make them promising for implementation into mobile devices for range-finding.

pMUT rangefinders were developed after bulk piezoelectric ultrasonic rangefinders, and the last decade witnessed the rapid development of pMUT rangefinders. At first, a single pMUT device with an AlN-based circular membrane was used to form a pMUT rangefinder system in 2010 [33]. After that, pMUT rangefinders with pMUT arrays, different types of pMUT device structures, and piezoelectric materials were developed to enhance the performance of pMUT rangefinder systems [34]. In addition to the advancements of pMUT devices, different range-finding methods are proposed [35]. Furthermore, various derivative systems based on pMUT rangefinders have been demonstrated, such as target positioning and object detection systems [16]. pMUT rangefinders are promising but still relatively new.

The main purpose of this article was to provide a state-of-the-art review of rangefinders based on pMUTs and a future outlook as well. Section 2 explains the principle of pMUT

rangefinders and analyzes the performance of pMUT rangefinders. Section 3 reviews how the performance of pMUT rangefinders has improved through the advancement of pMUT devices. Section 4 reviews advanced pMUT rangefinders based on improving the ranging method. Section 5 briefly introduces derivative systems of pMUT rangefinders. Section 6 summarizes this work and provides future outlooks of pMUT rangefinders.

2. Principle of pMUT Rangefinders

The working principles of pMUT rangefinders and the main factors affecting their performance are analyzed in this section to provide a foundation for pMUT rangefinder mechanism analysis and performance evaluation. In Section 2.1, the working mechanism and the signal propagation process of pMUT rangefinders are described. In Section 2.2, the analysis of pMUT rangefinder performance is given, and a quantitative relationship between the range and range error that determines the performance of pMUT rangefinders is deduced. After that, the main factors affecting the performance of pMUT rangefinders are analyzed in Section 2.3.

2.1. The Working Mechanism of pMUT Rangefinders

The block diagram of a pMUT rangefinder system is shown in Figure 2, where an electric transmitting signal from a signal generator is converted to an acoustic signal by the transmit mode of a pMUT device (①). The acoustic signal is reflected by the target (②), received by the receive mode of the pMUT device (③), which is converted back to the electric form (④) and picked up by an oscilloscope (⑤). Finally, the target range is given by data processing (⑥).

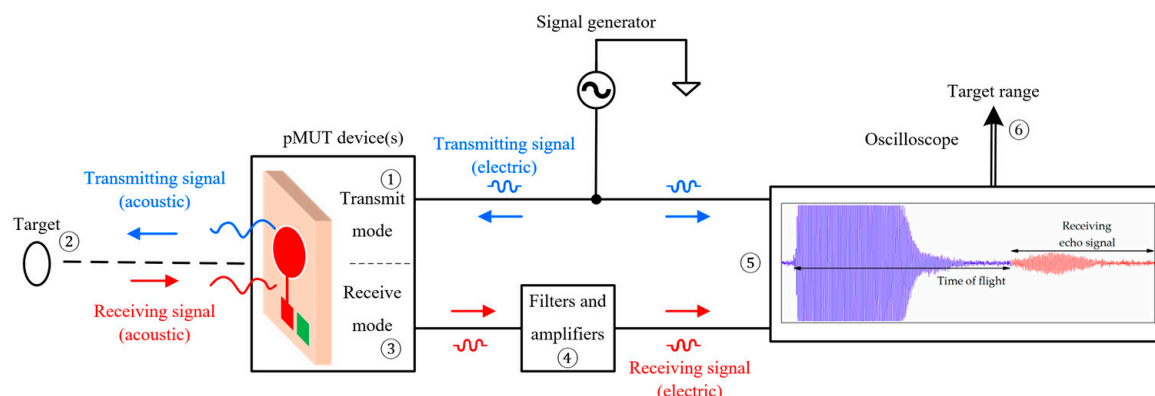


Figure 2. Block diagram of a pMUT rangefinder system. The signal shown in the oscilloscope is from [36] (Reproduced with permission from [36], Copyright 2018, MDPI AG).

For traditional pMUT rangefinder systems, a single circular pMUT device is used to transmit and receive signals with a working frequency f , where the waveforms of the transmitting and receiving signals are pulses and echoes, and the system is based on the time-of-flight (TOF) method (also named the pulse-echo method) to find the range of the target. The threshold TOF method is the most commonly used one for pMUT rangefinders due to its simple implementation, where the TOF is measured by the time interval between the starting point and the time at which the leading edge of the echo reaches the amplitude threshold [37], as shown in Figure 3. The range between the pMUT and the target is given by [38]

$$R = \frac{c \cdot \text{TOF}}{2} \quad (1)$$

where c is the sound speed.

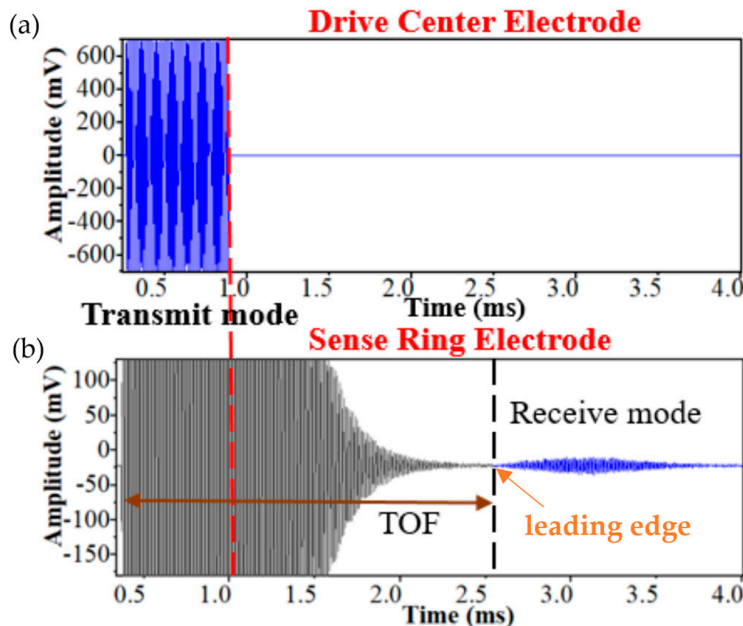


Figure 3. Illustration of the threshold TOF method. (a) The transmitting signals. (b) The receiving signal. Reproduced with permission from [39], Copyright 2019, IEEE.

Let us look at the signal propagation processes. The acoustic surface pressure amplitude P_{tx} generated by the transmit mode of the pMUT is proportional to the driving voltage V_d to excite the transmission mode of the pMUT, i.e.,

$$P_{tx} = G_t V_d \quad (2)$$

where G_t is the transmitting sensitivity of the pMUT. The signal is spread spherically, reflected by the target, and received by the pMUT. For far-field radiation, when acoustic absorption is neglected, the on-axis acoustic pressure function $p(r, t)$ at a distance r from a circular-membrane pMUT and a time, t , is given by [4,40,41]

$$p(r, t) = j\rho_{ac}cu_0 \cdot \frac{R_0}{r} e^{-j(\omega t - kr)} \quad (3)$$

where j is the imaginary unit, ρ_{ac} is the mass density of the medium, u_0 is the average velocity of the membrane, R_0 is the Rayleigh distance, $\omega = 2\pi f$ is the angular frequency, and k is the wave number. In Equation (3), the amplitude of the term " $\rho_{ac}cu_0$ " is equal to P_{tx} [41]. Equation (3) is usually used to calculate the sound pressure level [4] or the transmitting sensitivity [42] of a pMUT in its transmit mode since P_{tx} in Equation (2) is not directly measurable and must be derived using Equation (3). For the cases in which acoustic absorption is not neglectable (e.g., in-air range-finding) and the acoustic gain G_{ac} , which is related to the target geometry [31], must be considered, Equation (3) is changed to:

$$p(r, t) = j\rho_{ac}cu_0 \cdot \frac{R_0}{r} G_{ac} e^{-\alpha r} e^{-j(\omega t - kr)} \quad (4)$$

where α is the absorption coefficient, which is used to evaluate the energy losses along the acoustic propagation path in the medium. Note that α is dependent on the properties of the medium, including the viscosity, thermal conductivity, mass density, etc., and is positively related to the ultrasound frequency [43].

Due to the round-trip propagation between the pMUT and the target, the amplitude of the received pressure at the pMUT, P_{rx} , is obtained by setting $r = 2R$ in Equation (4), where R is the target range, i.e.,

$$P_{rx} = P_{tx} \frac{R_0}{2R} G_{ac} e^{-2\alpha R} \quad (5)$$

The received acoustic signal is converted to the electric signal by the pMUT in the receive mode, and the received voltage is given by:

$$V_{rx} = G_r P_{rx} \quad (6)$$

where G_r is the receiving sensitivity of the pMUT. The signal propagation processes are listed in Table 1 in order.

Table 1. The signal form alternation during the signal propagation process.

| Number | Signal Transmission Process | Corresponding Signals |
|--------|---|--|
| ① | Acoustic pressure generated by the pMUT transmit mode | $P_{tx} = G_t V_d$ |
| ② | Acoustic pressure received | $P_{rx} = P_{tx} \frac{R_0}{2R} G_{ac} e^{-2\alpha R}$ |
| ③ | Electric signal generated by the pMUT receive mode | $V_{rx} = G_r P_{rx}$ |

The relationship between the transmitting and receiving signals is described by Equations (2), (5) and (6), which will be used to analyze the performance of a pMUT rangefinder.

2.2. The Performance Evaluation of pMUT Rangefinders

A pMUT rangefinder is used for range-finding, so the maximum measurement range, R_{max} , is the main criterion to evaluate its performance. Meanwhile, with the increase in the target range, the received pressure P_{rx} is reduced and V_{rx} is decreased as well, according to Equations (5) and (6), and the accuracy of the range detection and the reliability of the range-finding result is lowered. Therefore, both R_{max} and the range-finding accuracy must be considered for the performance comparison of different pMUT rangefinders.

The range-finding accuracy of a pMUT rangefinder is determined by multiple aspects, including V_{rx} , noises and interferences, the bandwidth, and the range-finding method. A large receiving signal amplitude makes the feature points, especially the leading edge, clearer, so the TOF determination and range detection can be more accurate. V_{rx} is related to both the electrical and acoustic energy conversion processes according to Equations (2) and (6). With the increasing distance of the target, V_{rx} or P_{rx} decreases due to two main effects: one is that the signal is spread spherically and only a very small fraction of the energy is reflected by the target and received by the pMUT, and the other is acoustic absorption in the medium, according to Equation (5). Noises and interferences in a pMUT rangefinder system blur the signal and thus reduce the range-finding accuracy. Primary noises and interferences include the thermal noise caused by the random motion of the medium molecules received by the pMUT, the thermal noise of the piezoelectric element, the noises from the receiver circuit, the crosstalk between adjacent pMUT elements, the environmental reflections, and the possible multipath fading if the signal is continuous [44–46]. The signal-to-noise ratio (SNR) describes and evaluates the effects of V_{rx} as well as the noise and interference level on the accuracy. Combining Equations (2), (5) and (6) with the definition of SNR produces [37]:

$$SNR = \frac{\mathcal{S}}{\mathcal{N}} = \frac{\frac{1}{2} V_{rx}^2}{\frac{V_d^2}{2n^2}} = \frac{V_d^2}{2n^2} \cdot (G_t G_r G_{ac} R_0)^2 \cdot \frac{e^{-4\alpha R}}{4R^2} \quad (7)$$

where S is the signal power, \mathcal{N} is the noise power, and $\bar{n^2}$ is the mean-square of the noise voltage. Apart from the factors described by SNR, the range-finding accuracy is also affected by the pMUT bandwidth (BW) and the range-finding method. Ideally, the receiving signal is not spread and/or distorted compared to the transmitting signal, and the feature points, such as the leading edge, are sharp. However, due to the narrowband frequency response of the pMUT's membrane [11], the rise and fall times of the receiving signal depend on the BW, and the feature point positioning error is introduced by the reduction in the signal rise and fall slope. In addition, pMUT rangefinder systems using different range-finding methods have different signal waveforms or the methods to derive the target range from the signals are different, so the accuracies of the ranging results are not the same. To include those multiple aspects influencing the range-finding accuracy, a range error is defined and commonly used for range-finding accuracy evaluation [37]. For the threshold TOF method, which is the most commonly used for pMUT range-finding, the root-mean-square (RMS) range error, δ_R , is given by [47]

$$\delta_R = \frac{c}{2BW} \frac{1}{(2 \cdot SNR)^{\frac{1}{2}}} \quad (8)$$

In this paper, the RMS range error is abbreviated as the range error. The accuracy of a pMUT rangefinder system is revealed by its maximum range error δ_{Rmax} . Overall, in this paper, the maximum range R_{max} and the maximum range error δ_{Rmax} are mainly considered to evaluate the performance of pMUT rangefinders.

In Equation (8), the bandwidth for a single-mode membrane is given by $BW = \frac{f_0}{Q}$, where f_0 is the resonant frequency and Q is the quality factor [48,49]. Combining Equations (7) and (8) produces:

$$\delta_R = \frac{Q \cdot c \cdot \sqrt{\bar{n^2}}}{G_t G_r G_{ac} R_0 f_0 V_d} \cdot R \cdot e^{2\alpha R} \quad (9)$$

According to Equations (7) and (9), when R increases, SNR almost exponentially decreases while δ_R almost exponentially increases. This prediction is in good agreement with the experimental results of pMUT rangefinders, as shown in Figure 4. If the range error is large, the range-finding result given by the pMUT rangefinder is inaccurate. Plugging δ_{Rmax} and R_{max} into Equation (9) yields

$$\delta_{Rmax} = \frac{Q \cdot c \cdot \sqrt{\bar{n^2}}}{G_t G_r G_{ac} R_0 f_0 V_d} \cdot R_{max} \cdot e^{2\alpha R_{max}} \quad (10)$$

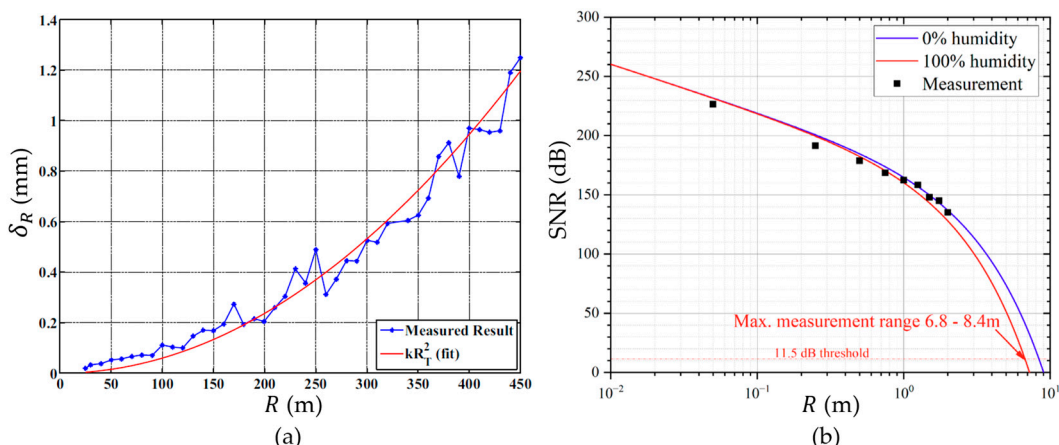


Figure 4. (a) δ_R versus R . Reproduced with permission from [33], Copyright 2010, IEEE. (b) SNR versus R . Reproduced with permission from [31], Copyright 2022, MDPI AG.

When δ_R is required to be less than the maximum allowed range error δ_{Rmax} , the R_{max} that a pMUT rangefinder can achieve is determined by multiple factors that will be discussed in Section 2.3.

2.3. Main Factors Affecting pMUT Rangefinder Performance

According to Equation (10) and the previous analysis, with the enhancements of G_t and G_{ac} , an increased R_{max} can be achieved with fixed δ_{Rmax} , where G_{ac} is related to the target size and the directivity that can be changed by different pMUT structures [50], PCB baffle sizes [51], etc. A commonly used way to increase G_{ac} by making the signal more directional is to add a horn on the pMUT [52]. In addition, with the increase in G_r , the receiving electric signal amplitude is increased with the side effect that the noise caused by the acoustic thermal noise is also increased. However, since acoustic noise is only one of the noise sources, the SNR is still largely increased with the enhancement of G_r and thus R_{max} can be increased accordingly. G_t , G_r , and G_{ac} can be enhanced by the pMUT device improvement.

Admittedly, the R_{max} can be increased or the δ_{Rmax} can be decreased by increasing the value of the driving voltage V_d according to Equation (10). However, higher driving voltage means higher power consumption and even nonlinearity [13], so both high performance and a moderate driving voltage should be achieved. In addition, the R_{max} is positively related to the Rayleigh distance R_0 with a fixed δ_{Rmax} in Equation (10), and R_0 is given by [40]:

$$R_0 = \frac{A}{\lambda} = \frac{fA}{c} \quad (11)$$

where A is the membrane surface area, λ is the wavelength, and f is the frequency of the signal transmitted by the pMUT and is referred to as the working frequency in this paper. According to the above equation, increasing A leads to a higher Rayleigh distance R_0 , and thus a larger R_{max} with fixed δ_{Rmax} , but the size and power consumption of the pMUT are also increased, and the resonant frequency is changed as well [53]. Therefore, the strategy to enhance the performance by directly changing the membrane area is rarely adopted.

Some factors have dual effects on the performance that should be properly designed, including the quality factor Q . Firstly, the increase in Q causes a decrease in the bandwidth, so R_{max} is decreased or δ_{Rmax} is increased, according to Equation (10). Secondly, the transmitting and receiving sensitivities G_t and G_r are also relevant to Q . A high Q means low acoustic and structural damping of pMUTs [54]. Therefore, with the increase in Q , the energy conversion efficiency is increased, and G_t and G_r are enhanced. Because of the dual effects of Q on the parameters of pMUTs, Q should be designed to be a moderate value to balance the high bandwidth and high sensitivity requirements for lower range error and larger detection range.

The working frequency f and the resonant frequency f_0 also have multiple effects on pMUT rangefinder performance. f is the actual frequency of the pMUT driving signal while f_0 is a property of the pMUT and is determined by the pMUT material and structure. In most pMUT rangefinder systems, to ensure the maximum vibration of the pMUT membrane, f should be set as approximately equal to f_0 [15]. The signal amplitude reduction due to the difference between f and f_0 causes the increase in δ_{Rmax} or decrease in R_{max} . According to Equation (10), for media with high absorption, the primary effect of f is acoustic absorption. An example of the relationship between the transmission loss and the range in a spread-only situation without absorption and in acoustic absorption situations with different frequencies is shown in Figure 5. With the decrease in f , the absorption coefficient α is decreased [40], so the transmission loss is reduced, and the R_{max} is increased with fixed δ_{Rmax} . In addition, with the reduction in f , the electric and mechano-acoustic impedances are decreased, so the receiving sensitivity G_r can be enhanced [54]. However, f should not be too low because the Rayleigh distance R_0 is decreased with f reduction according to Equation (11), resulting in a higher range of error. Furthermore, since f_0 should be close to f , with small f , the pMUT device has to be redesigned to have lower f_0 , which in

turn causes lower bandwidth and higher range error. In addition, the quality factor Q may be also altered with the change in f_0 [55]. Therefore, multiple effects of f and f_0 must be considered during the design of the pMUT in order to obtain the optimal frequency of the pMUT rangefinder system in different scenarios. For the in-air range-finding, the working frequency should be moderately low due to the large absorption of air. For instance, a pMUT rangefinder first achieving more than a five-meter detection range with over 11.5 dB SNR was proposed by Yang et al. [31], where the working frequency was 66 kHz, which is lower than most previous designs. For in-liquid range-finding, the acoustic absorption is low, and the working frequency is usually in the MHz range [46] for higher bandwidth and larger Rayleigh distance.

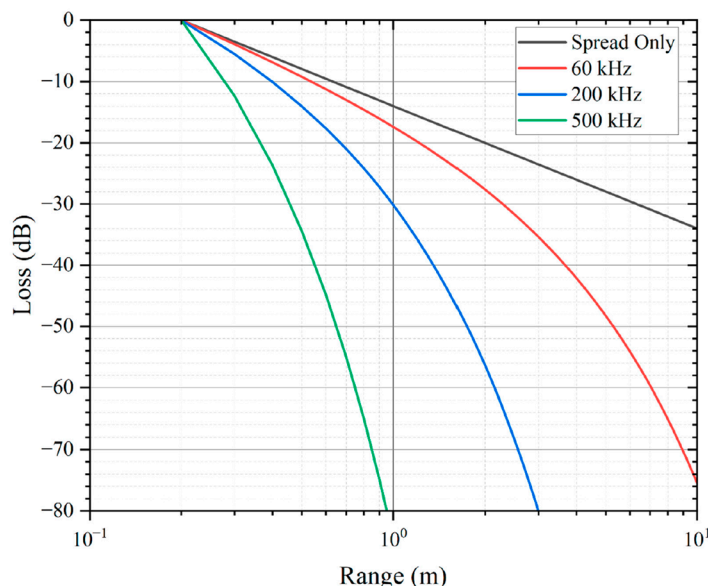


Figure 5. The transmission loss in a spread-only situation without absorption and in-air absorption situations with different frequencies at 20 °C and 50% air humidity. Reproduced with permission from [31], Copyright 2022, MDPI AG.

The mean-square of the noise voltage $\overline{n^2}$ and the absorption coefficient α negatively affect pMUT rangefinder performance. $\overline{v_n^2}$ is determined by the noise and interference sources from the pMUT rangefinder and environment that are discussed in Section 2.2. α is determined by the working frequency f and properties of the medium that are discussed in Section 2.1. The reduction in $\overline{n^2}$ and/or α gives rise to higher R_{max} or lower δ_{Rmax} , according to Equation (10).

Overall, Table 2 lists the main factors affecting pMUT rangefinder performance and the trends of the maximum range R_{max} with the increase in those factors when the maximum range error δ_{Rmax} is fixed. Some of the factors could be improved by employing advanced pMUT devices and range-finding methods. Strategies to improve pMUT devices and range-finding methods for high-performance pMUT rangefinders are analyzed in detail in Sections 3 and 4, respectively.

Table 2. Main factors that affect the performance of pMUT rangefinders.

| Name | Symbol | Main Effect * |
|--------------------------------------|----------|---|
| The driving voltage | V_d | $R_{max} \uparrow$ |
| The working frequency | f | Dual effects ** |
| The resonant frequency | f_0 | $BW \uparrow \rightarrow R_{max} \uparrow^{**}$ |
| The transmitting sensitivity | G_t | $R_{max} \uparrow$ |
| The receiving sensitivity | G_r | $R_{max} \uparrow$ |
| The acoustic gain | G_{ac} | $R_{max} \uparrow$ |
| The quality factor | Q | Dual effects |
| The surface area of the membrane | A | $R_{max} \uparrow$ |
| The mean-square of the noise voltage | n^2 | $R_{max} \downarrow$ |
| Absorption coefficient | α | $R_{max} \downarrow$ |

* “↑” means that the increase in this factor will enhance the parameter, and “↓” means that the increase in this factor will lower the parameter. ** f should be approximately equal to f_0 to achieve the maximum vibration, so their effects are not independent.

3. Advancements of pMUT Rangefinders Based on Improvements of pMUT Devices

A typical pMUT rangefinder system is made of a single pMUT device with a circular membrane and uses AlN as the piezoelectric material. This type of pMUT rangefinder has limited performance. In order to achieve the higher performance pMUT rangefinder systems, pMUT arrays, advanced pMUT device structures, and novel piezoelectric materials have been applied to pMUT rangefinders, which are discussed in detail in this section.

3.1. pMUT Rangefinders with pMUT Arrays

Using pMUT arrays to substitute a single pMUT for range-finding can help to achieve a higher maximum range or lower range error. As more pMUT elements are used for signal transmitting and receiving, the total transmitting and receiving acoustic signal amplitude are manyfold increased, so the SNR is increased, and the range error is largely reduced [13]. In addition, pMUT arrays with more element numbers can help to improve the directivity [56,57], so more acoustic energy is transmitted along the direction of the target and thus the receiving signal is enhanced, which in turn improves the maximum range and reduces the range error. In addition, since less energy along other directions is spread, the environmental reflection that affects the noise level is reduced, and thus \bar{n}^2 is lowered, as discussed in Section 2.2. For a one-dimensional (1D) array, assuming that the directivity with a single pMUT element is one, the directivity function $D(\theta)$ with an array of pMUT elements is given by [58]

$$D(\theta) = \frac{\sin\left(\frac{\pi N d}{\lambda} \sin \theta\right)}{N \cdot \sin\left(\frac{\pi d}{\lambda} \sin \theta\right)} \quad (12)$$

where N is the number of elements, d is the spacing between adjacent elements, and θ is the azimuth. The directivity function is represented by the normalized sound pressure and is shown in Figure 6. According to Figure 6, with the increase in the element number, the width of the main lobe is decreased, which means that the directivity is improved. The theory is also valid for two-dimensional (2D) arrays [59].

The types of pMUT array structures include line arrays (1D arrays) [60,61], polygon (e.g., hexagon) arrays [62,63], and square arrays [55,64], as shown in Figure 7. In many rangefinder systems using pMUT arrays, in order to keep the transmitter electrodes and the receiver electrodes in the same vibrational mode, respectively, all the transmitter electrodes are connected by metal bridges, and all the receiver electrodes are connected as well [65,66].

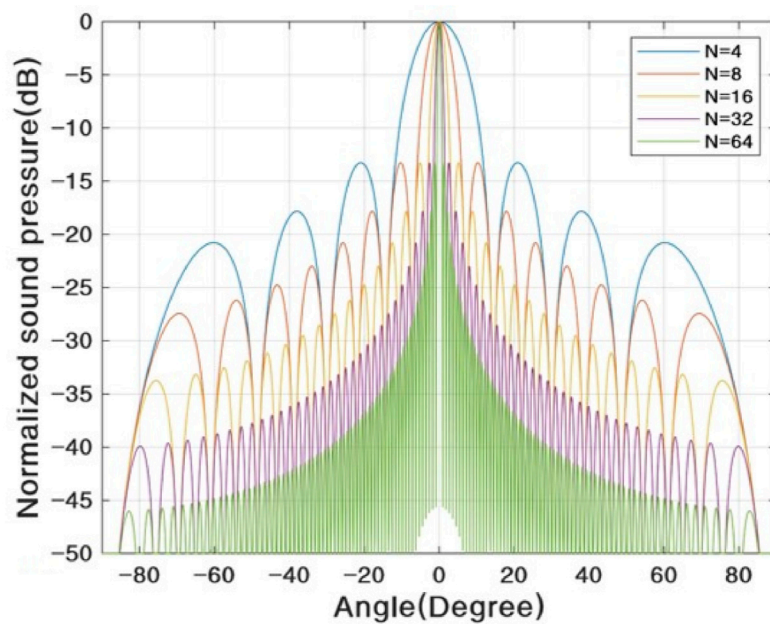


Figure 6. The influence of the element number on the directivity. Reproduced with permission from [58], Copyright 2022, MDPI AG.

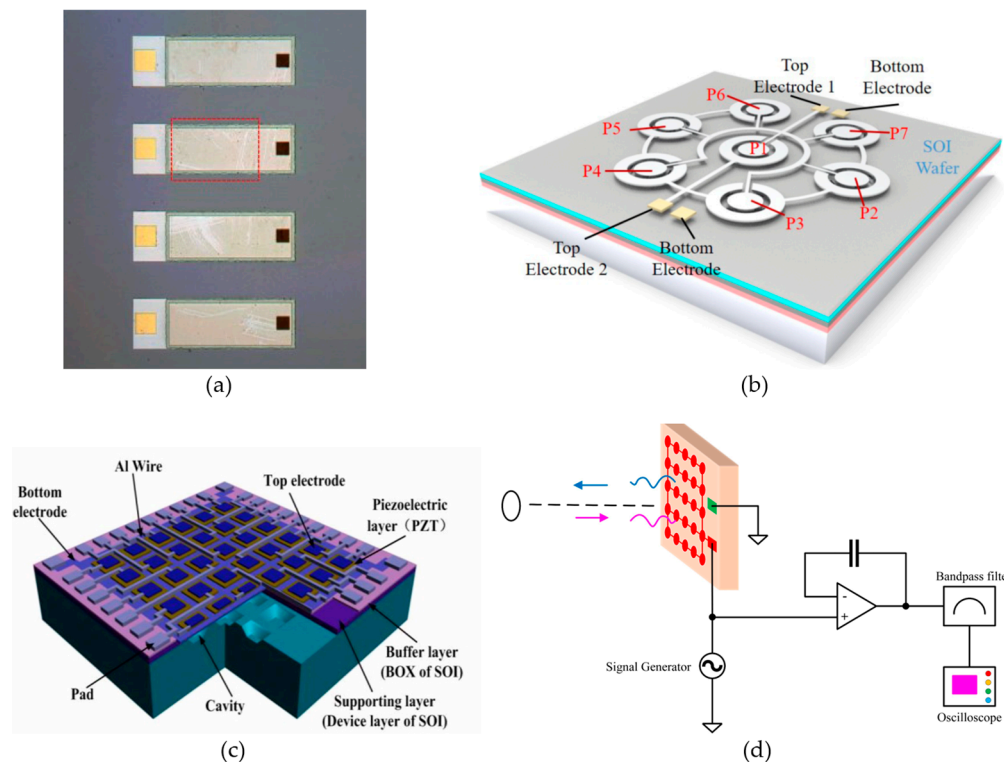


Figure 7. (a) A 1D pMUT array. Reproduced with permission from [61], Copyright 2016, IEEE. (b) A hexagonal pMUT array. Reproduced with permission from [62], Copyright 2021, IEEE. (c) A 2D square array. Reproduced with permission from [23], Copyright 2013, MDPI AG. (d) A pMUT rangefinder system using a pMUT array.

Advanced pMUT array designs can improve the factors affecting pMUT performance, in which the density of pMUT elements and the mechanical or acoustic crosstalk between pMUT elements must be considered. By increasing the density of pMUT elements, the transmitting and receiving signal amplitude per unit area is enhanced. However, when

reducing the spacing between pMUT elements to increase the element density, the crosstalk or cross-coupling between different elements must be carefully considered [23]. Strategies for minimizing the pMUT array crosstalk have been developed. For example, Yang et al. analyzed the mutual-coupling effect with different spacings in a square array of pMUTs and figured out the optimal spacing under a certain working frequency [23]. Moreover, Xu et al. proposed a resonant cavity design for a pMUT array to reduce crosstalk [67]. Vysotskyi et al. overviewed and compared acoustic isolation techniques for pMUT arrays concerning crosstalk reduction [68].

Table 3 lists the parameters of pMUT rangefinders with a single pMUT or different pMUT arrays. According to Table 3, pMUT arrays with large numbers of elements generally have high maximum ranges or high accuracies, which accords with the analysis. Note that the examples listed in Table 3 have different structures, piezoelectric materials, driving voltages, and δ_{Rmax} or SNR_{min} . Thus, more control experiments of range-finding using single pMUTs and pMUT arrays with different element numbers need to be carried out in the future to further evaluate the contribution of pMUT arrays on the performance enhancement of pMUT rangefinder systems.

Table 3. Summary of a single pMUT rangefinder or rangefinder arrays with different element numbers.

| Element Number | R_{max} (m) ** | δ_{Rmax} (mm) ** | SNR_{min} | V_d (V) | f (kHz) | f_0 (kHz) | Ref. |
|-----------------------|------------------|-------------------------|------------------|-----------|-----------|-------------|------|
| 1 element | 0.45 | 1.3 | — | 6.5 | 214 | 214 | [69] |
| 7 receiver elements * | 0.75 | 3.5 | 28 dB (at 0.5 m) | 15 | — | 190 | [52] |
| 7 elements | 0.5 | ~0.67 *** | — | 5 | — | 77.34 | [62] |
| 4 elements | 2.4 | — | 12 dB | 5 | ~48 | — | [70] |
| 14 elements | 6.8 | — | 11.5 dB | 5 | 66 | 66 | [31] |

* [52] used a line of seven elements in an array as the receiver units. ** All the ranges and the corresponding range errors that were measured by the distance between the transmitter and the receiver were then divided by two to be converted to the reflection mode results for performance comparison. *** The range error reported in [62] is seen as the 3σ error, which is divided by three to be converted to the RMS errors and then divided by two to be converted to the reflection mode results in this paper.

3.2. pMUT Rangefinders with Advanced pMUT Device Structures

In addition to using pMUT arrays to enhance range-finding performance, pMUT rangefinders with advanced device structures have been exploited as well. For instance, some key parameters, including the transmitting and receiving sensitivities, are improved by optimizing the membrane shape of pMUT devices. Most conventional pMUT rangefinders use circular membrane pMUTs; nonetheless, some pMUT rangefinder designs have adopted square membranes for pMUTs recently, as shown in Figure 8. The vibrational modes of a pMUT are determined by the shape of the piezoelectric membrane, as shown in Figure 9. For the same device size, square-membrane pMUT units have a higher coverage area than circular ones [42], so the membrane vibration displacement of square-membrane pMUTs is largely higher than circular ones with the same driving voltage, which is proved by a comparison experiment in [71], as shown in Figure 10. Therefore, square membrane pMUT rangefinders have the potential for higher sensitivities G_t and G_r than current circular ones and achieve a larger detection range and lower range error. Chiu et al. reported a square-membrane pMUT rangefinder system [72] that achieved a higher maximum range (0.5 m) and lower range error (0.63 mm) than a comparable circular-membrane pMUT rangefinder (0.45 m maximum range with 1.3 mm error) [33]. In the future, the square-membrane pMUT structure may be combined with other strategies to further enhance pMUT rangefinder performance.

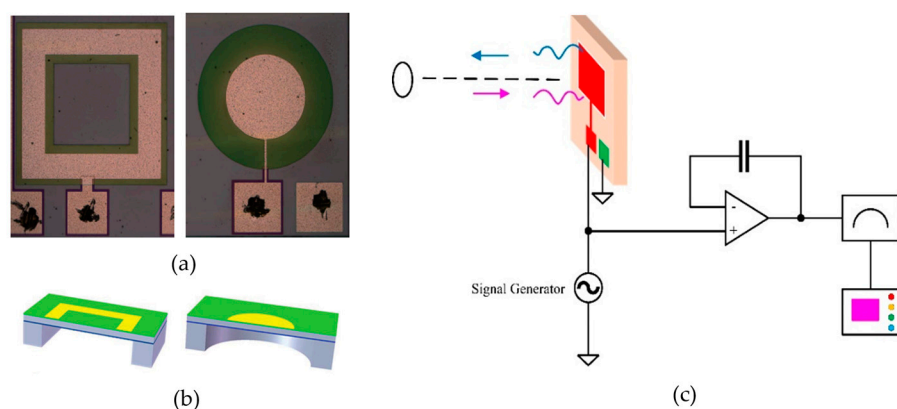


Figure 8. (a) Comparison between the structure of a square-membrane pMUT (left) and a circular-membrane pMUT (right). Reproduced with permission from [71], Copyright 2018, IEEE. (b) A 3D model of square- and circular-membrane pMUTs. Reproduced with permission from [71], Copyright 2018, IEEE. (c) A pMUT rangefinder system using a square-membrane pMUT.

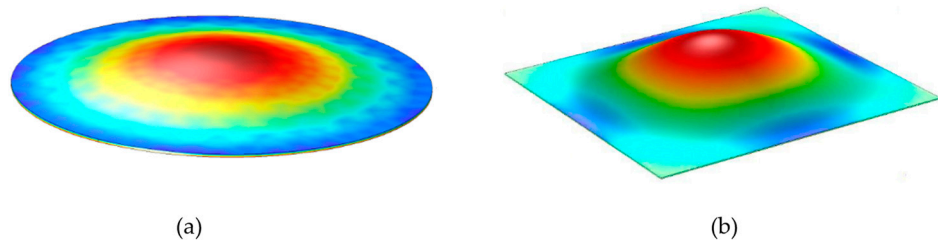


Figure 9. (a) The shape of deflection of a circular membrane. Reproduced with permission from [39], Copyright 2019, IEEE. (b) The shape of deflection of a square membrane. Reproduced with permission from [36], Copyright 2018, MDPI AG.

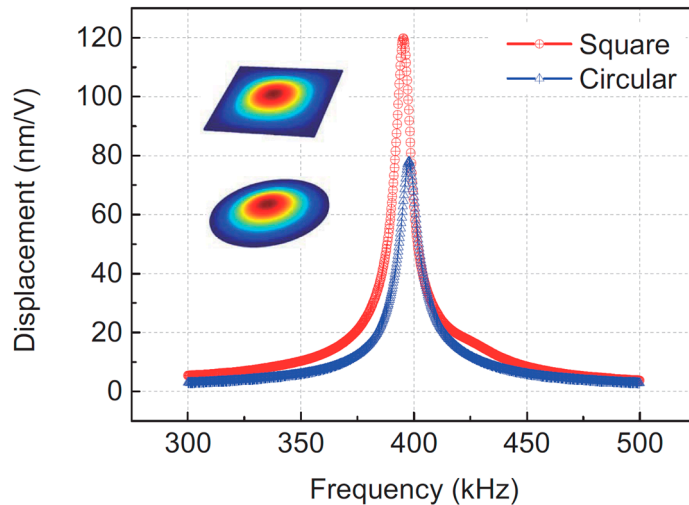


Figure 10. Tested vibration displacements of square- and circular-membrane pMUTs. Reproduced with permission from [71], Copyright 2018, IEEE.

Apart from the membrane shape change, Zhou et al. proposed a dual-electrode pMUT rangefinder system [15], as shown in Figure 11a. The pMUT transmitter has both inner and outer electrodes, and the driving electric signals of the electrodes have a 180° -phase difference. The electrodes with anti-phase driving signals control the displacement field of the membrane and improve the transmitting sensitivity. Therefore, the output acoustic pressure of the dual-electrode mode transmitter with anti-phase driving signals is considerably higher than the single electrode one, as shown in Figure 11b. Range-finding

experiments were carried out, and the rangefinder system in the dual-electrode mode exhibited a 2.2 m maximum distance (i.e., a 1.1 m maximum range in the reflection target detection), which is 29.4% larger than the single electrode mode.

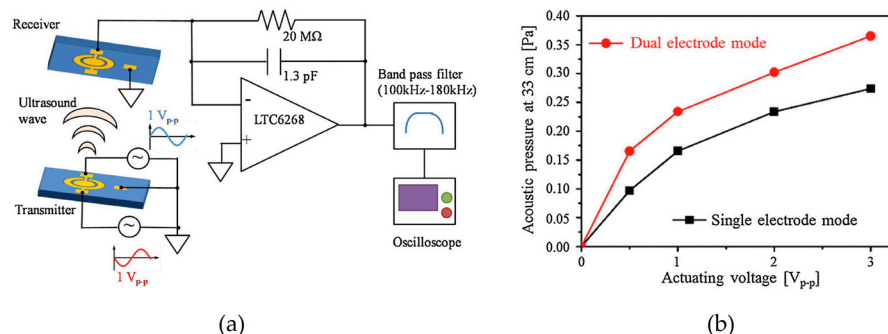


Figure 11. (a) A pMUT rangefinder using a dual electrode transmitter driven by anti-phase electric signals. (b) The relationship between the acoustic pressure and the driving voltage in dual electrode and single electrode modes. Reproduced with permission from [15], Copyright 2017, Elsevier B.V.

There are other advanced pMUT device structures that are promising to be used for high-performance range-finding. For example, a bimorph structure is an effective way for pMUTs to enhance sensitivities, where the membrane of a pMUT contains two piezoelectric layers [73,74]. Because the number of piezoelectric layers is doubled, the vibration displacement and acoustic pressure of bimorph pMUTs are much larger than those of unimorph ones [75]. Shao et al. utilized a bimorph structure and developed a pMUT rangefinder derivative system to detect a target over 1 m away with a more than $\pm 65^\circ$ field of view [76], which was greater than the $\pm 45^\circ$ field of view of a unimorph design [13]. Moreover, other advanced structure designs, including the venting structure [50], dome shape [77], and unclosed membrane [78], may be further explored in order to extend the maximum range and lower the range error of pMUT rangefinders in the future.

Table 4 lists the parameters of typical pMUT rangefinders with different structures found in the literature. The maximum ranges and range errors of these pMUT rangefinders will also be illustrated in Figure 12.

Table 4. Summary of pMUT rangefinders with different device structures.

| Structure Features | R _{max} (m) * | δR _{max} (mm) * | SNR _{min} | V _d (V) | f (kHz) | f ₀ (kHz) | Ref. |
|--|------------------------|--------------------------|--------------------|--------------------|---------|----------------------|------|
| Circular membrane | 0.45 | 1.3 | — | ~5.9 | 214 | 214 | [33] |
| Circular membrane | 0.65 | ~0.28 ** | ~27.5 dB | 13 | — | 215 | [11] |
| Square membrane | 0.5 | 0.63 | — | 1.8 | 97 | 97, 96 | [72] |
| Square membrane | 1.4 | — | ~0 dB | — | 29 | 33 | [36] |
| Dual electrode with anti-phase driving signals | 1.1 | — | 12 dB | 0.5 | — | 154 | [15] |

* All the ranges and the corresponding range errors that were measured by the distance between the transmitter and the receiver are divided by two to be converted to the reflection mode results for performance comparison. ** The 3σ error in [11] is divided by three to be converted to the RMS error and then divided by two to be converted to the reflection mode result.

3.3. pMUT Rangefinders with Novel Piezoelectric Materials

The transmitting sensitivity G_t and the receiving sensitivity G_r are mainly dependent on the piezoelectric materials of pMUT devices [79]:

$$\begin{cases} G_t \propto |e_{31,f}| \\ G_r \propto \frac{|e_{31,f}|}{\varepsilon_0 \varepsilon_{33}} \end{cases} \quad (13)$$

where $e_{31,f}$ is the piezoelectric constant, ϵ_0 is the vacuum permittivity, and ϵ_{33} is the relative dielectric constant in the z-direction. Therefore, the product of the sensitivities $G_t G_r$ can be described by $\frac{e_{31,f}^2}{\epsilon_0 \epsilon_{33}}$, which is denoted as the figure of merit for a pMUT [80]. Since larger $G_t G_r$ give rise to a smaller maximum range error $\delta_{R_{max}}$ or larger maximum range R_{max} according to Equation (10), researchers have been working on choosing different piezoelectric materials and strategies to enhance $G_t G_r$ by increasing the absolute value of $e_{31,f}$ or decreasing ϵ_{33} in order to enlarge the maximum range of pMUT rangefinders [81–83].

ZnO [84], PZT [85–87], and AlN [88–90] are widely used materials for pMUT devices with the advancement of thin-film deposition technologies. The drawback of ZnO is that it has a relatively high conductivity [91]. A PZT-based pMUT rangefinder has higher G_t due to its high piezoelectric coefficients, but its G_r is limited because of its high dielectric constants, so the $G_t G_r$ or $\frac{e_{31,f}^2}{\epsilon_0 \epsilon_{33}}$ of PZT is not largely higher compared to that of AlN, as shown in Table 5 [92,93]. Furthermore, AlN is more compatible with CMOS fabrication than ZnO and PZT, which enables AlN pMUT rangefinders to be integrated in chips [92,94]. Overall, AlN is the most commonly used material for pMUT rangefinders.

However, AlN-based pMUT rangefinders have limited performance due to their low piezoelectric coefficients $e_{31,f}$ and high sensitivity to parasitic capacitance [91]. Since conventional PZT-based pMUTs cannot replace AlN-based pMUT rangefinders for their poor G_r , as it has been explained above, researchers applied various strategies to improve PZT films for advanced pMUT rangefinders with performance surpassing current AlN-based ones [95]. For example, S. Yoshida et al. developed a monocrystalline $Pb(Mn_{1/3},Nb_{2/3})O_3$ -PZT (PMnN-PZT) epitaxial thin film pMUT rangefinder [15]. According to Table 5, PMnN-PZT has a higher $\frac{e_{31,f}^2}{\epsilon_0 \epsilon_{33}}$, so it has a large $G_t G_r$. Therefore, the maximum range of PMnN-PZT pMUT rangefinders is increased to 2.2 m, i.e., 1.1 m in the reflection mode. Another example is the design of the single-crystal-PZT pMUT rangefinder developed by Luo et al. in 2020 [70], which has a maximum range of 2.4 m in the reflection mode. The $\frac{e_{31,f}^2}{\epsilon_0 \epsilon_{33}}$ of single-crystal PZT is not only obviously higher than conventional PZT but is also more than that of PMnN-PZT, according to Table 5. Furthermore, the single-crystal-PZT pMUT rangefinder in [70] has lower resonant frequencies (40~50 kHz) than the PMnN-PZT (>150 kHz) rangefinder in [15]. Since moderately low resonant frequencies are favorable for in-air pMUT rangefinders with long-range detection according to Section 2.3, the single-crystal-PZT-based pMUT rangefinder in [70] achieves higher R_{max} .

Table 5. Comparison of piezoelectric materials for pMUT rangefinders. Reproduced with permission from [70], Copyright 2021, IEEE.

| Materials | $e_{31,f}$ ($C \cdot m^2$) | ϵ_{33} | $\frac{e_{31,f}^2}{\epsilon_0 \epsilon_{33}}$ (Gpa) |
|-------------------------|------------------------------|-----------------|---|
| AlN [96,97] | −1 | 10 | 10.8 |
| PZT (2 μm) [27] | −13.1 | 854 | 22.7 |
| PMnN-PZT [15] | −14 | ~250 | 88.6 |
| Single-crystal PZT [70] | −16~−24 | 308 | 93.7~211 |
| 20% ScAlN [98,99] | −1.6 | 12 | 24.1 |

Apart from totally changing the piezoelectric material from AlN to other ones, other research has focused on doping AlN with suitable materials such as Scandium (Sc) to achieve a high piezoelectric coefficient [100,101]. This strategy balances the objectives that keep the advantages of AlN and increase the absolute value of $e_{31,f}$. Yang et al. demonstrated a pMUT rangefinder array based on AlScN film, and a long-range detection with a maximum range of 6.8 m and $SNR \geq 11.5$ dB was achieved [31].

Table 6 lists the parameters of pMUT rangefinders with different piezoelectric materials. According to Table 6, pMUT rangefinders based on PMnN-PZT, single-crystal PZT, and AlScN were observed to have obviously higher detection ranges than those on AlN

and PZT. In particular, the AlScN pMUT rangefinder reaches the largest detection range (6.8 m), and the PMnN-PZT pMUT rangefinder in [15] realizes a long-range measurement of 1.1 m with very low power consumption (0.5 V driving voltage and about 16 μ W), while a counterpart AlN pMUT rangefinder needs 10 V to reach the comparable R_{max} .

Table 6. Summary of pMUT rangefinders with different piezoelectric materials.

| Piezoelectric Material | R_{max} (m) * | $\delta_{R_{max}}$ (mm) * | SNR_{min} | V_d (V) | f (kHz) | f_0 (kHz) | Ref. |
|------------------------|-----------------|---------------------------|-------------|-----------|-----------|-------------|-------|
| AlN | 0.45 | 1.3 | — | 6.5 | 214 | 214 | [69] |
| PZT | 0.0175 | 0.1225 ** | — | 1.5 | ~30 | ~30 | [102] |
| PMnN-PZT | 1.1 | — | 12 dB | 0.5 | — | 154 | [15] |
| Single-crystal PZT | 2.4 | — | 12 dB | 5 | ~48 | — | [70] |
| AlScN | 6.8 | — | 11.5 dB | 5 | 66 | 66 | [31] |

* All the ranges and the corresponding range errors that are measured by the distance between the transmitter and the receiver are divided by two to be converted to the reflection mode results for performance comparison.

** The error was less than 0.7% in [102], so $\delta_{R_{max}}$ of [102] was estimated by 0.7% R_{max} .

The performances of TOF pMUT rangefinders with different pMUT devices are collectively presented in Figure 12. Note that for the performance comparison between two individual rangefinders, both R_{max} and $\delta_{R_{max}}$ must be considered at the same time. For instance, the one with the same $\delta_{R_{max}}$ but higher R_{max} , or the one with the same R_{max} but lower $\delta_{R_{max}}$, or the one with a higher R_{max} and lower $\delta_{R_{max}}$ has a higher performance. In the figure, the colors of the markers stand for the working frequency f (f is substituted by the resonant frequency f_0 for those pMUT rangefinders that did not explicitly provide f , and f is averaged for those with multiple working frequencies), \circ is a circular membrane pMUT, and \diamond is a square membrane pMUT. The hollow markers \bullet and \blacklozenge refer to those with no pMUT arrays used, while the solid markers \bullet and \blacklozenge refer to those with pMUT arrays as transmitters and/or receivers. Those pMUT rangefinders that used piezoelectric materials other than AlN are labeled. It can be seen in Figure 12 that moderately low working frequencies are desirable for pMUT rangefinders to achieve long-range detection, and the suitable working frequency range is approximately 40~200 kHz. Employing piezoelectric materials with high piezoelectric constants in pMUTs is the most effective means of extending the maximum range. In addition, pMUT arrays also contribute to the range error reduction or the maximum range enlargement. Square-membrane pMUT rangefinders have larger maximum ranges than their circular membrane counterparts, although the number of reported square-membrane pMUT rangefinders is relatively small.

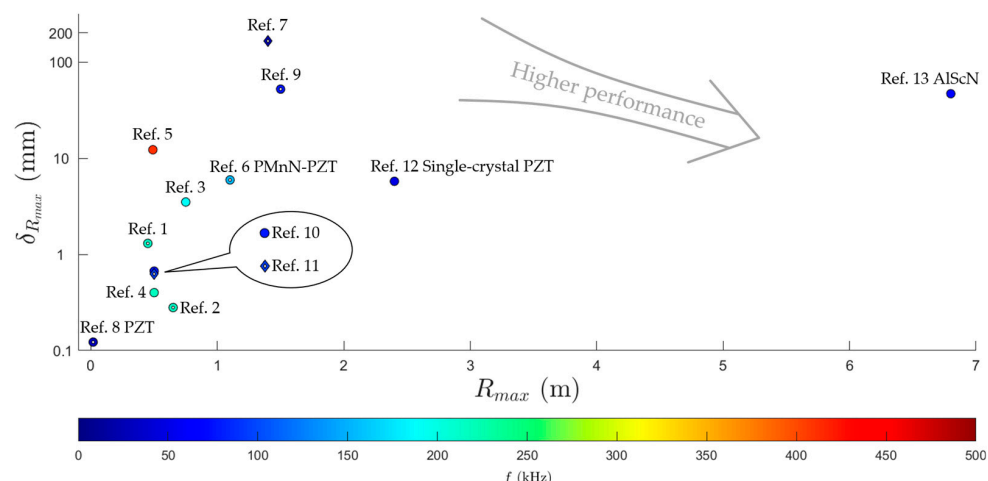


Figure 12. Performance comparison illustration of different TOF pMUT rangefinders. All the ranges and the corresponding range errors that are measured by the distance between the transmitter and

the receiver are divided by two to be converted to the reflection mode results for performance comparison. 3σ errors are divided by three to be converted to the RMS errors. For those pMUT rangefinders that did not report their maximum range errors, δ_{Rmax} is estimated by Equation (8), where the sound speed is set to be $c = 343$ m/s according to [103]. Data are from Ref. 1 ([33]), Ref. 2 ([11]), Ref. 3 ([52]), Ref. 4 ([13]), Ref. 5 ([55]), Ref. 6 ([15]), Ref. 7 ([36]), Ref. 8 ([102]), Ref. 9 ([39]), Ref. 10 ([62]), Ref. 11 ([72]), Ref. 12 ([70]), and Ref. 13 ([31]) in published year sequence.

4. Advancements of pMUT Rangefinders Based on Improvements of Range-Finding Methods

Section 3 describes the ways to enhance the performance of pMUT rangefinder systems by improving pMUT devices. Another form of performance enhancement is the improvement of the range-finding method. pMUT range-finding systems based on advanced TOF range-finding methods achieve high accuracy and wide detection range in long-range detection and are analyzed in Section 4.1. pMUT range-finding systems based on continuous wave (CW) range-finding methods achieve high accuracy in short-range detection and are analyzed in Section 4.2.

4.1. Advanced Time-of-Flight Range-Finding Methods for pMUT Rangefinders

4.1.1. TOF with Cross Correlation for Enhanced Accuracy

According to Section 2.1, traditional TOF pMUT rangefinder systems only use a single point to calculate the range, which may have a large range error because the attenuated received signals combined with considerable noises and interferences obscure the position of the leading edge. To address this problem, a cross-correlation TOF system was proposed, where signals were sampled, cross-correlation was performed, and the whole envelopes of the transmitting and receiving signals were compared and calibrated to determine the time of flight. Sampling sequences of the transmitting and receiving signals were cross-correlated [104], and the lag of the maximum cross-correlation peak, τ_{max} , was given. Then, the distance between the transmitter and receiver, L , was given by [19,105]

$$L = \left(\frac{\tau_{max}}{f_s} - \text{TOE} \right) c - L_{cal} \quad (14)$$

where f_s is the sampling frequency, TOE is the time of the emission of the signal, and L_{cal} is a calibration constant. The range R between the pMUT rangefinder and the target can be obtained by combining Equation (14) with $R = L/2$.

In the cross-correlation method, the range result is determined not only by one point but by multiple feature points on the envelope, so the random noise can be mitigated and n^2 , in Equation (10), can be decreased, resulting in a lower range error and higher accuracy. Furthermore, in order to diminish the envelope distortion during energy conversion processes, the envelope shape of the transmitting signal in this system can be well designed to have enough smooth rising and falling slopes, as well as containing enough feature points [33]. A practical design of the envelope shape and the diagram of a pMUT rangefinder system applying the cross-correlation TOF method is shown in Figure 13 [33].

R. Przybyla et al. developed the first pMUT rangefinder system based on the cross-correlation TOF method as early as 2010 [33]. Many recent works also use cross correlation to obtain the detection range [31,106].

4.1.2. TOF with Ring-Down Suppression for Lower Blind Area

The maximum range is often the main parameter to be enhanced in most research on pMUT rangefinders in order to make pMUT rangefinders more competitive and to be applied to commercial range-finding use. Nevertheless, some recent research demonstrated strategies to lower the minimum detectable range. TOF pMUT rangefinder systems with a single pMUT device have a relatively large minimum detectable range due to the ring-down effect of the vibrating membrane, as shown in Figure 14. The ring-down effect is the

main cause to extend the blind area of a pMUT rangefinder because the signal received during the ring-down stage is overlapped or distorted by the ring-down vibration, where the range error is largely increased, and the range-finding may fail [107]. The minimum detectable range of a TOF pMUT rangefinder can be defined by the blind area duration.

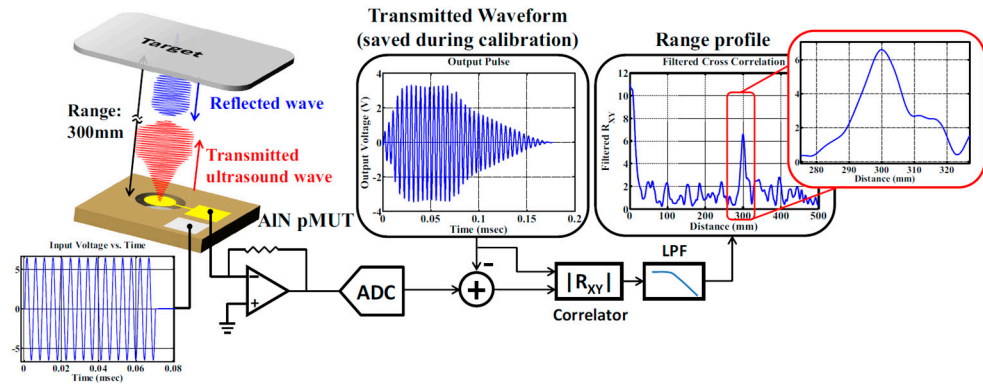


Figure 13. Block diagram of a pMUT rangefinder system using the cross correlation TOF method. Reproduced with permission from [33], Copyright 2010, IEEE.

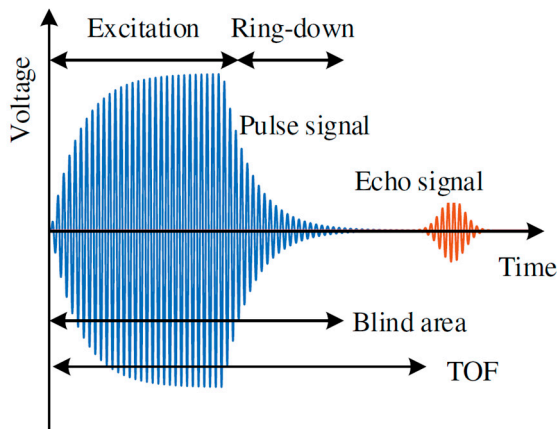


Figure 14. Illustration of the ring down of a pMUT rangefinder. Reproduced with permission from [107], Copyright 2021, MDPI AG.

A simple way to avoid the blind area is to use two pMUT devices that are physically separated, where one of the pMUTs always works at the TX mode and the other always at the RX mode. However, the device size, readout circuit, and power consumption are largely increased if doubling the number of pMUT devices. Another strategy to lower the minimum detectable range in relatively short-range detection for pMUT rangefinders working in switching TX and RX modes is to redesign the transmitting signal to suppress the ring-down effect and reduce the blind area. For instance, Pala et al. proposed a method of ring-down suppression [108], in which the transmitting signal consisted of a number (N_p) of normal cycles, such as the excitation signal and a number (N_n) of cycles that are 180° phase-shifted as the suppression signal, as shown in Figure 15a. The normal cycle and the 180° phase-shifted cycle signals counteract the vibration of the pMUT membrane and accelerate the vibration attenuation so that the ring-down time is reduced. The number of cycles N_p and N_n must be properly determined. When N_n is not large enough, the counteracting effect is not adequate, while when N_n is too high, the additional 180° phase-shifted signal over-acts and excites the vibration of the pMUT membrane in its phase and frequency. In the experiment of [108], the optimal choice is $N_p = 10$ and $N_n = 6$, as shown in Figure 15b, and the minimum detectable range (the blind area) is reduced from 13.91 cm to 12.16 cm. Furthermore, Wu et al. demonstrated a transfer function-based ring-down suppression method [107], which also achieved ring-down reduction through excitation

signal suppression, but the suppression signal waveform was improved, as shown in Figure 15c, where the suppression signal was generated by a system including a transfer function and a simple proportion controller. The comparison experiment was carried out, and the minimum range (the blind area) was reduced by about 40% [107], as shown in Figure 15d. In the future, accuracy experiments of the ring-down suppression methods should be carried out to obtain the range error or SNR of the pMUT rangefinders using the methods in order to evaluate the accuracy of those methods in relatively short range detection compared with other designs.

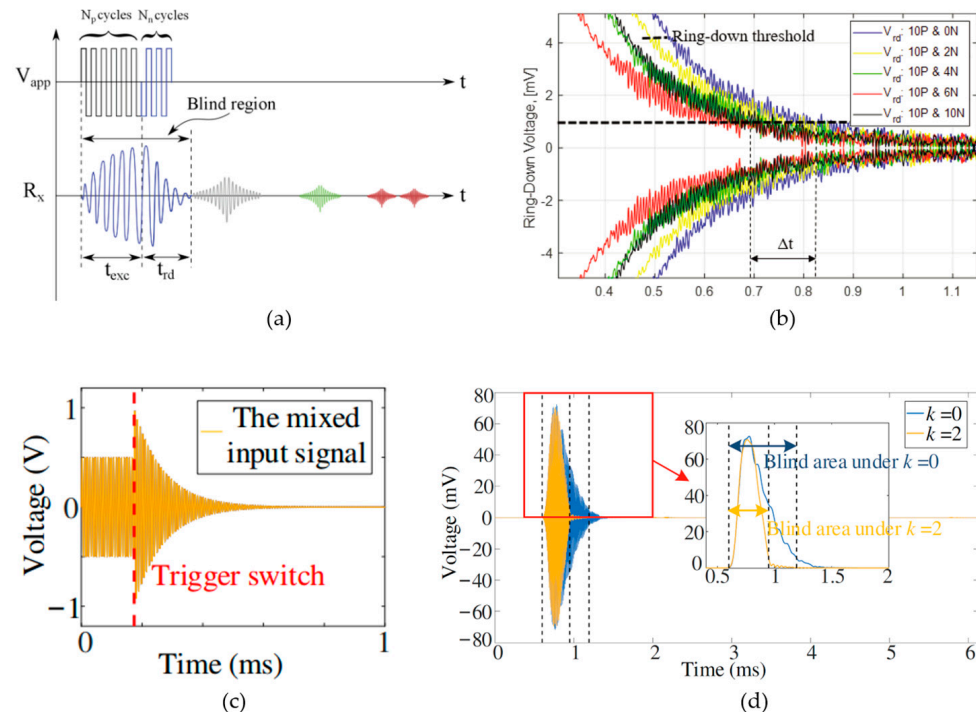


Figure 15. (a) Illustration of the 180° phase-shift ring-down suppression method [108]. Reproduced with permission from [108], Copyright 2021, IEEE. (b) The comparison experiment before and after suppression in [108]. Reproduced with permission from [108], Copyright 2021, IEEE. (c) The suppression signal of the ring-down suppression method is in [107]. Reproduced with permission from [107], Copyright 2021, MDPI AG. (d) The comparison experiment before and after suppression in [107]. Reproduced with permission from [107], Copyright 2021, MDPI AG.

4.2. Advanced Continuous Wave Range-Finding Methods for pMUT Rangefinders

4.2.1. MFCW pMUT Rangefinder System

The accuracy of TOF-based pMUT rangefinders is largely limited by the receiving signal amplitude which is heavily reduced by acoustic absorption [109]. Different from TOF methods that obtain the target range by amplitude information, continuous wave (CW) methods obtain the range by phase difference information, so they can achieve a higher accuracy than TOF methods [35]. Unlike TOF methods that the signals are pulses and echoes, CW methods transmit and receive continuous wave signals to find the range. The vibration modes of the signals in CW methods are steady, so they are less affected by bandwidth limitations. The change in the range-finding method from TOF methods to CW methods changes the relationship between δ_R and SNR [47], so the δ_R can be reduced even if V_d and \bar{n}^2 are not changed.

The simplest CW-based pMUT rangefinder system is to only use a sinusoidal wave as the signal. The phase detector can detect the phase difference between the transmitting

and receiving signals, $\Delta\varphi$. The range is half of the distance L between the transmitter and the receiver and is given by [110]:

$$R = \frac{L}{2} = \frac{c\Delta\varphi}{4\pi f} \quad (15)$$

where f is the frequency of the signal. However, since $\Delta\varphi \leq 2\pi$, $R \leq \frac{c}{2f_0}$, so $R_{max} = \frac{c}{2f_0}$, which is very small. If the range is more than $\frac{c}{2f_0}$, phase ambiguity will occur. The simplest CW-based system cannot be used for pMUT rangefinders due to their low detection range. To address the problem of the detection range limitation, two frequency continuous wave (TFCW) systems have been proposed, where the signal contains two sinusoidal waves with slightly different frequencies f_1 and f_2 ($|f_1 - f_2| = \Delta f$), so the range is given by [111]:

$$R = \frac{L}{2} = \frac{c\Delta\varphi}{4\pi\Delta f} \quad (16)$$

Since $\Delta\varphi \leq 2\pi$, $R_{max} = \frac{c}{2\Delta f}$, so R_{max} is increased. The range error of a TFCW system is given by [47]:

$$\delta_R = \frac{c}{2\pi \cdot BW} \frac{1}{(2 \cdot SNR)^{\frac{1}{2}}} \quad (17)$$

By comparing Equations (8) and (17), the range error of a TFCW system is π times lower than a threshold TOF system with the same SNR, bandwidth, and sound speed. However, there is a trade-off between R_{max} and δ_{Rmax} for the TFCW system. Although δ_R is decreased with the increase in Δf , R_{max} is shortened when Δf is increased. To balance the parameters, R_{max} cannot be too high and δ_{Rmax} cannot be too low.

To solve this problem, multi-frequency continuous wave (MFCW) pMUT rangefinder systems are proposed, where three sinusoidal waves with frequencies of f_1 , f_2 , and f_3 are transmitted simultaneously ($f_1 > f_2 > f_3$). Define that $\Delta f_{i,j} = f_i - f_j$ is the frequency difference between the i th and j th waves, φ_i is the phase shift of the i th wave when it arrives at the receiver, and $\Delta\varphi_{i,j} = \varphi_i - \varphi_j$ is the phase shift difference between the i th and j th waves. The working mechanism of the MFCW method is illustrated in Figure 16, and the range R is given by [111]:

$$R = \frac{L}{2} = \frac{c}{2} \left(\text{Int} \left[\frac{\Delta\varphi_{1,2} \cdot \Delta f_{1,3}}{2\pi\Delta f_{1,2}} \right] \frac{1}{\Delta f_{1,3}} + \text{Int} \left[\frac{\Delta\varphi_{1,3} \cdot f_1}{2\pi\Delta f_{1,3}} \right] \frac{1}{f_1} + \frac{\varphi_1}{2\pi f_1} \right) \quad (18)$$

As long as $\Delta f_{1,3}$ is sufficiently larger than $\Delta f_{1,2}$, R_{max} can be nearly independently increased with the decrease in $\Delta f_{1,2}$, and the range error can be independently decreased with the increase in $\Delta f_{1,3}$ and f_1 , where $c/\Delta f_{1,3}$ determines the first-order resolution and c/f_1 determines the second-order resolution. Thus, R_{max} and δ_{Rmax} are separately controlled [35]. As phenomenologically illustrated in Figure 17, for a TFCW system, when the period of the envelope is extended from Figure 17(a1) to Figure 17(a2), R_{max} increases at the cost that the average slope of the envelope is also reduced, meaning that the resolution and the range error are decreased. In contrast, for an MFCW system, with the increase in the envelope's period from Figure 17(b1) to Figure 17(b2), R_{max} extends, and the average slope of the envelope (the spines with different heights) nearly does not change, which means that δ_{Rmax} is approximately not increased. Furthermore, since MFCW systems use phase, not time-of-flight, to calculate the range, they are less affected by the large amplitude attenuation of the signal, which further enhances the accuracy of MFCW pMUT rangefinder systems.

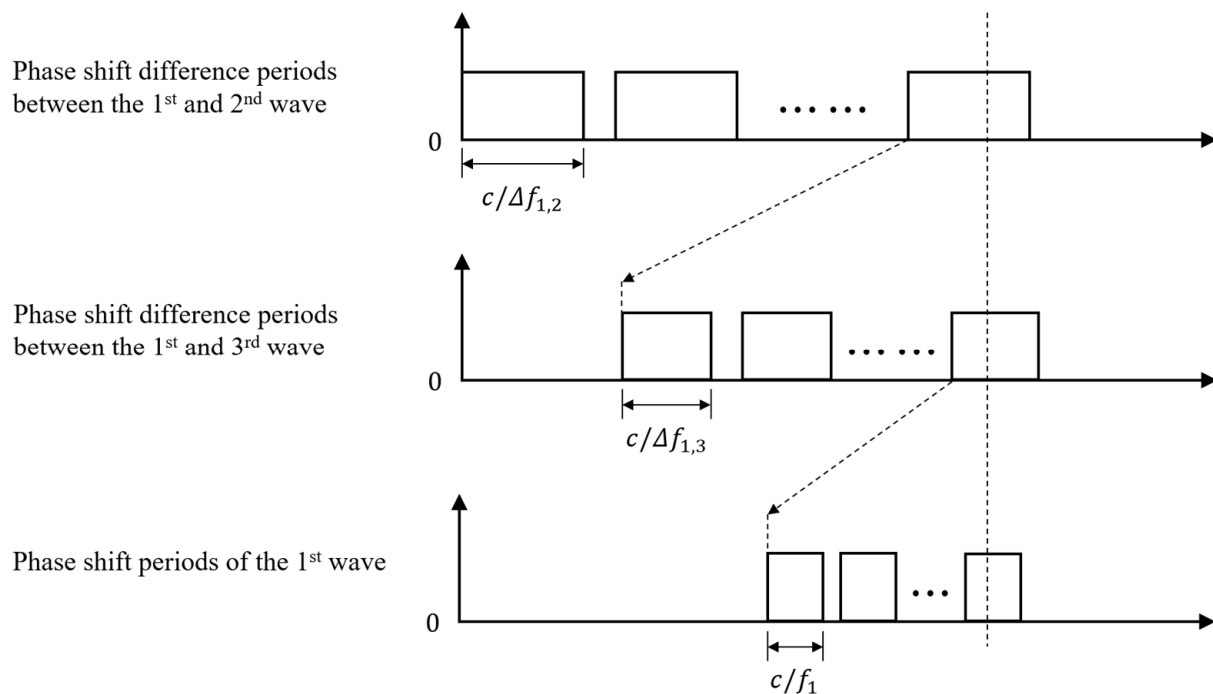


Figure 16. Illustration of the working mechanism of the MFCW method.

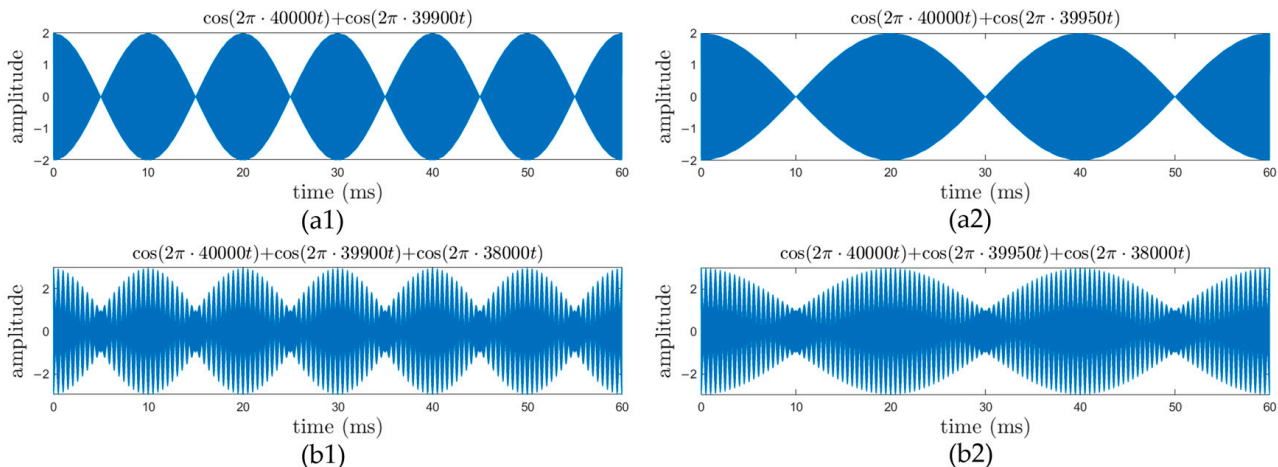


Figure 17. The illustration of TFCW waveforms (a1) Before period extension and (a2) After period extension, and MFCW waveforms (b1) Before period extension and (b2) After period extension.

In 2019, Chen et al. developed an MFCW-based pMUT rangefinder system and achieved a less than $0.0711 \text{ mm } 3\sigma$ error (i.e., $\delta_R < 0.024 \text{ mm}$) when $R < 0.1 \text{ m}$ (for most TOF-based pMUT rangefinder systems, δ_R are not less than 0.4 mm) [35]. Although the detection range of this MFCW-based system is relatively low due to the maximum range limitation, MFCW-based pMUT rangefinder systems are promising to be used for high-accuracy short-range detection. The block diagram of an MFCW pMUT rangefinder system is shown in Figure 18. Different from a TOF system, the waveform generator must output three continuous waves with different frequencies [35].

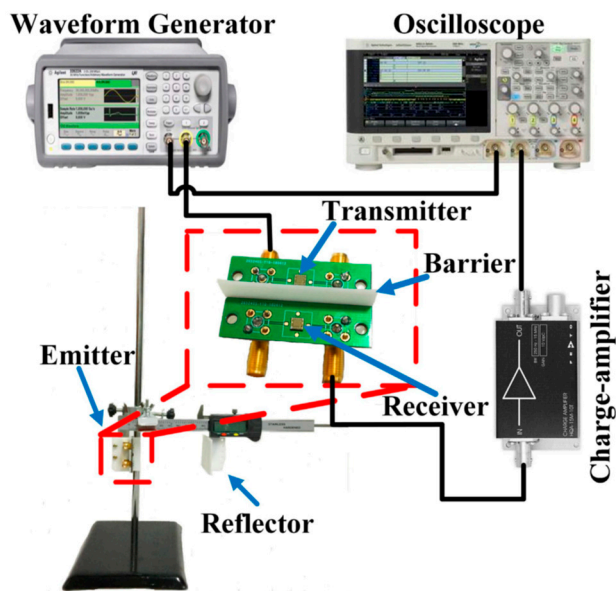


Figure 18. Block diagram of a MFCW pMUT rangefinder system. Reproduced with permission from [35], Copyright 2019, IEEE.

Table 7 lists the typical rangefinders with continuous wave methods. According to Table 7, MFCW rangefinders have larger R_{max} and lower δ_{Rmax} than the TFCW one. The conventional transducer-based range finder has a higher R_{max} than the pMUT-based one, which means that the performance of the pMUT rangefinder should further be improved in the future to be competitive for commercial use.

Table 7. Summary of rangefinders with continuous wave methods.

| Device | Method | R_{max}/m * | δ_{Rmax}/mm * | Wave Frequencies | Ref. |
|--|--------|---------------|---|--|-------|
| Conventional ultrasonic transmitter and receiver | TFCW | 0.1 | 1.5 | 39.85 and 40.6 kHz | [112] |
| Conventional ultrasonic transducers | MFCW | 0.75 | 0.052 | 40, 39.9, 38.0 kHz | [111] |
| pMUTs | MFCW | 0.3 | ~0.024 for $R < 0.1$ m, ~0.61 for 0.1–0.3 m ** | 497, 496.8, 487 kHz for $R < 0.1$ m 492, 491.8, 490 kHz for 0.1–0.3 m | [35] |

* All the ranges and the corresponding range errors that were measured by the distance between the transmitter and the receiver were divided by two to be converted to the reflection mode results for performance comparison.

** The 3σ errors in [35] are divided by three to be converted to the RMS errors.

4.2.2. MFPW pMUT Rangefinder System

MFCW-based pMUT rangefinder systems cannot achieve ideally high performance due to multipath reflections that are caused by the standing waves formed between the pMUT device and the target [45]. To eliminate this side effect, Zamora et al. proposed a novel system configuration for pMUT rangefinders named a multi-frequency pulsed wave (MFPW) system in 2021 [46], where three continuous waves are replaced by three pulses, each of which contains a single sinusoidal wave with several cycles. Additionally, the number of cycles, as well as the interval between distinct pulses, are well designed to make different pulses distinguishable and have a time-of-flight that is more than the total length of the transmitted signal, as shown in Figure 19. φ_1 , φ_2 , and φ_3 are measured from these three pulses, respectively, and then $\Delta\varphi_{1,2}$ and $\Delta\varphi_{1,3}$ can be determined. The following steps to derive the range are similar as in the MFCW system described above. An MFPW system has a similar calculation process as an MFCW system, but it avoids interferences caused by multipath fading because discontinuous signals cannot form standing waves. The pMUT

rangefinder system in [46] has an extremely low error: lower than 6.2 μm within a 3.5 mm transmitter-receiver distance.

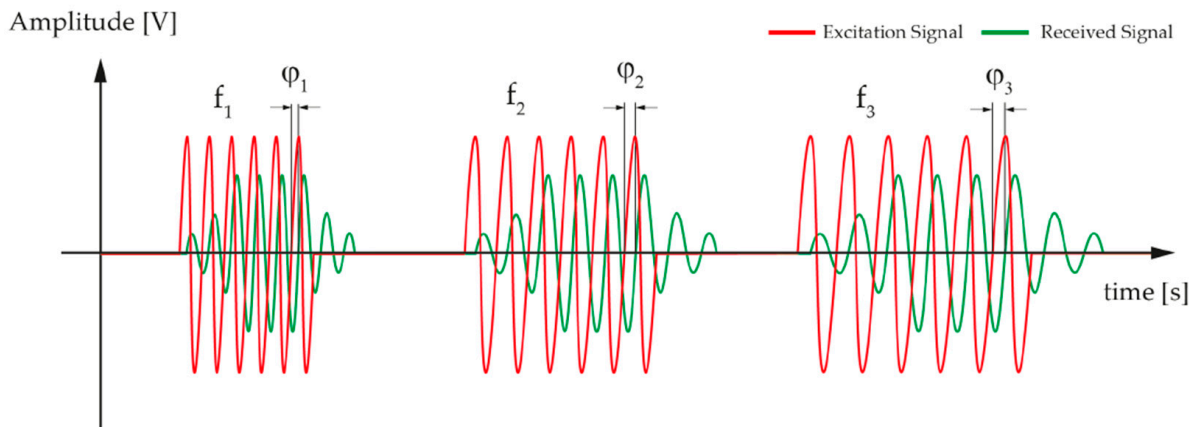


Figure 19. Illustration of the MFPW method. Reproduced with permission from [46], Copyright 2021, MDPI AG.

MFCW- and MFPW-based pMUT rangefinder systems are suitable to measure a short range (<several decimeters) because the R_{max} is limited by the maximum phase shift difference of 2π . However, MFCW- and MFPW-based pMUT rangefinder systems have shown their extremely low range error when the range is short. Thus, they are competitive for short-range detection with high accuracy.

Overall, there are various kinds of pMUT rangefinder systems that are used for different applications. For long-range detection ($>1 \text{ m}$), pMUT rangefinder systems should have moderately low working frequency according to Section 2.3 and utilize TOF range-finding methods. For short-range detection ($<0.1 \text{ m}$) with the low-range-error requirement, pMUT rangefinder systems should utilize MFCW or MFPW range-finding methods.

5. Derivative Systems of pMUT Rangefinders

pMUT rangefinders described in Sections 2–4 can only find the range of a target but not the angle and direction of the target. Nevertheless, a group of pMUT rangefinders can be combined as an array to accomplish more complicated tasks such as target positioning (Section 5.1) and object detection (Section 5.2). These systems are named derivative systems of pMUT rangefinders because they are not simply pMUT rangefinder systems but are extensions of pMUT rangefinder systems.

5.1. pMUT Rangefinder Derivative Systems for Target Positioning

A pMUT rangefinder target positioning system can determine the position of a single point in a space so that the range and the angles of the point in a spherical coordinate frame can be measured. A target positioning system consists of $N \times N$ pMUT elements that are independently wired, and the time-of-flight of each element, τ_{ij} , is separately calculated. For a target with the azimuths of θ and φ , the differences in the time-of-flight between neighboring elements of the pMUT array are given by [52]

$$\begin{cases} \Delta\tau_x = \frac{d}{c} \sin\theta \cdot \sin\varphi \\ \Delta\tau_y = \frac{d}{c} \sin\theta \cdot \cos\varphi \end{cases} \quad (19)$$

where d is the adjacent element spacing ($R \gg Nd$), $\Delta\tau_x$ is the difference in the time-of-flight between neighboring elements along the x-axis, and $\Delta\tau_y$ is that along the y-axis. d has to be designed to be smaller than $\lambda/2$ to avoid grating lobes [113]. The target range R can be directly obtained by the τ_{ij} data through Equation (1), and the azimuths θ and φ can be obtained by the known $\Delta\tau_x$ and $\Delta\tau_y$ data through Equation (19). Finally, the position of the target is given in Figure 20.

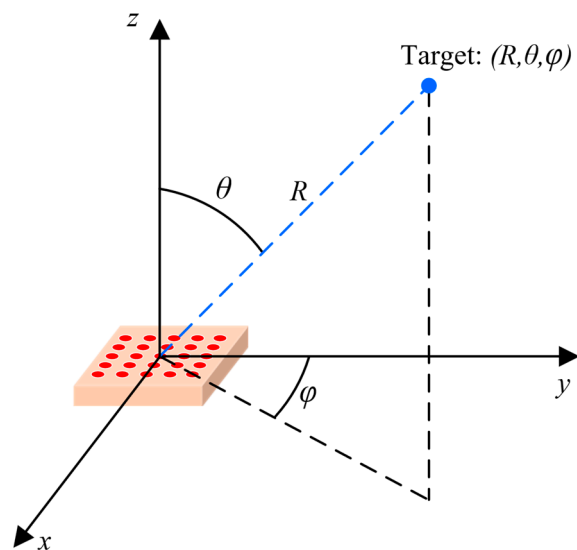


Figure 20. Illustration of a pMUT rangefinder target positioning system.

5.2. pMUT Rangefinder Derivative Systems for Object Detection

pMUT rangefinder arrays can be utilized for object detection as well, where a group of range data of the points of an object [76] or a hand [16] is measured by the pMUT rangefinder array before data processing is used to detect the presence of the object or recognize the object features. An example of a pMUT rangefinder object detection system for gesture recognition is shown in Figure 21a.

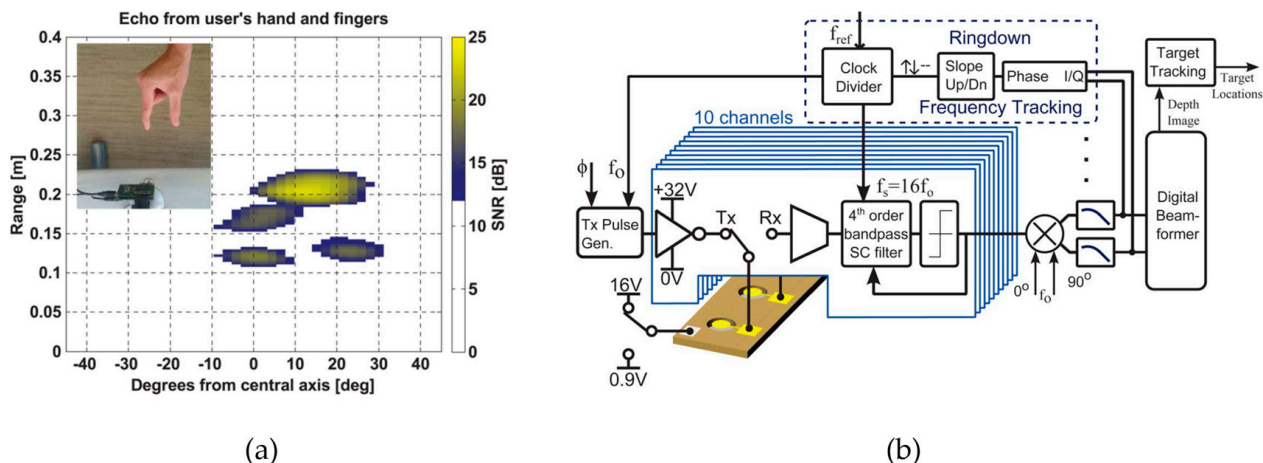


Figure 21. (a) A pMUT rangefinder object detection system for gesture recognition. (b) Block diagram of the pMUT rangefinder gesture recognition system. Reproduced with permission from [13]. Copyright 2015, IEEE.

Because of the narrowband property of pMUTs, all the elements in a pMUT rangefinder array for object detection have the same working frequency. A CMOS circuitry capable of demodulation, frequency tracking, pulse generation, beamforming, and target tracking should be integrated with a pMUT rangefinder array to construct the system [13], as shown in Figure 21b, where beamforming is the most crucial part. Without deliberate beamforming, the echo signals reflected by multiple points of a target or multiple targets mix and superpose together, so one cannot distinguish a range difference from an angular difference by analyzing the signal differences of distinct elements for a pMUT rangefinder array. Hence, beam steering must be added so that the pMUT array only detects the range of a point in a certain direction at a time and then scans the direction [114,115]. The

illustration of steering based on beamforming is shown in Figure 22. When measuring the range of target 1, phase delays are set to the elements of the pMUT array to compensate for the difference in the time-of-flight in the direction of target 1 (θ_1), and then the received signals are summed together. Consequently, the received signal from θ_1 is intensified, but other signals (e.g., in the direction of target 2 (θ_2)) are not, so the range obtained this time is the range of target 1.

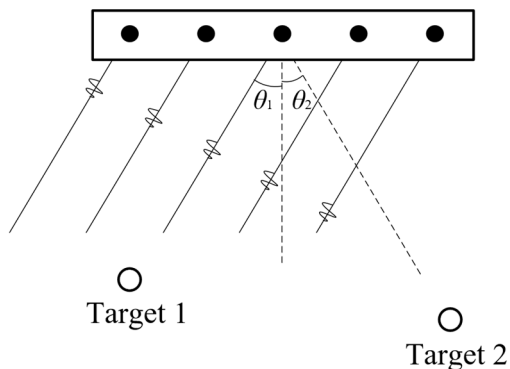


Figure 22. Illustration of steering during beamforming.

6. Summary and Future Outlooks

This article discusses piezoelectric micromachined ultrasonic transducers (pMUTs) for range-finding. A brief introduction of pMUT rangefinders has been given, including their basic structures, working principles, advantages, and applications. Various designs for high-performance pMUT rangefinders have been discussed. pMUT arrays as well as advanced device structures (e.g., bimorph structure) and piezoelectric materials (e.g., AlScN) help to achieve high performance. Additionally, advanced range-finding methods (e.g., the MFPW method) are able to enhance the range-finding accuracy as well. Moreover, derivative systems of pMUT rangefinders that extend the use of pMUT rangefinders are briefly introduced.

With the maturing of advanced pMUT devices, pMUT rangefinders are promising as replacements for bulk piezoelectric transducers for commercial mobile range-finding because of their small size, low cost, and low power consumption. The performance of pMUT rangefinder systems should be further improved to enable pMUT rangefinders to be competitive consumer devices. Specifically, two main aspects should be focused on in the future: (1) the narrowband property of pMUTs makes their bandwidth generally lower than their counterparts, especially cMUTs, so electric and acoustic signal conversion processes inevitably have heavy distortions, and pMUT rangefinders are not competent to high-resolution 3D range-finding detection, especially in the air. The structural design, materials, and fabrication techniques of pMUTs have to be improved to increase their bandwidth, which, unfortunately, has not been extensively researched now. (2) It is still challenging to enable pMUT rangefinders with small sizes to generate a high output pressure that is comparable to bulk rangefinders. Therefore, in the future, pMUT rangefinders should be continuously improved through a deeper understanding of their principles, innovative structures, and/or new materials to reach a comparable output pressure as bulk rangefinders. Furthermore, high-performance range-finding methods such as frequency modulation and binary modulation that have not been applied to pMUT rangefinders are prospective to be researched for pMUT rangefinder systems for a particular use. In conclusion, the future development of pMUT rangefinders is challenging but promising.

Author Contributions: Methodology, conceptualization, and editing, J.P. and H.X.; writing—original draft preparation and figures preparation, J.P. and C.B.; writing—review and editing, J.P., C.B., Q.Z. and H.X.; supervision and project administration, H.X.; funding acquisition, H.X. All authors have read and agreed to the published version of the manuscript.

Funding: This research was funded by the Foshan Science and Technology Innovation Project (2018IT100252).

Data Availability Statement: Not applicable.

Conflicts of Interest: The authors declare no conflict of interest.

References

- Qiu, Y.; Gigliotti, J.V.; Wallace, M.; Griggio, F.; Demore, C.E.; Cochran, S.; Trolier-McKinstry, S. Piezoelectric micromachined ultrasound transducer (PMUT) arrays for integrated sensing, actuation and imaging. *Sensors* **2015**, *15*, 8020–8041. [[CrossRef](#)] [[PubMed](#)]
- Nazemi, H.; Antony Balasingam, J.; Swaminathan, S.; Ambrose, K.; Nathani, M.U.; Ahmadi, T.; Yameema, B.L.; Emadi, A. Mass Sensors Based on Capacitive and Piezoelectric Micromachined Ultrasonic Transducers-CMUT and PMUT. *Sensors* **2020**, *20*, 2010. [[CrossRef](#)]
- Jiang, X.; Tang, H.Y.; Lu, Y.; Ng, E.J.; Tsai, J.M.; Boser, B.E.; Horsley, D.A. Ultrasonic Fingerprint Sensor With Transmit Beamforming Based on a PMUT Array Bonded to CMOS Circuitry. *IEEE Trans. Ultrason. Ferroelectr. Freq. Control* **2017**, *64*, 1401–1408. [[CrossRef](#)]
- Wang, H.; Ma, Y.; Zheng, Q.; Cao, K.; Lu, Y.; Xie, H. Review of Recent Development of MEMS Speakers. *Micromachines* **2021**, *12*, 1257. [[CrossRef](#)] [[PubMed](#)]
- Proto, A.; Rufer, L.; Basrour, S.; Penhaker, M. Modeling and Measurement of an Ultrasound Power Delivery System for Charging Implantable Devices Using an AlN-Based pMUT as Receiver. *Micromachines* **2022**, *13*, 2127. [[CrossRef](#)] [[PubMed](#)]
- Lu, Y.; Tang, H.; Wang, Q.; Fung, S.; Tsai, J.M.; Daneman, M.; Boser, B.E.; Horsley, D.A. Waveguide piezoelectric micromachined ultrasonic transducer array for short-range pulse-echo imaging. *Appl. Phys. Lett.* **2015**, *106*, 193506. [[CrossRef](#)]
- Lu, Y.; Tang, H.; Fung, S.; Wang, Q.; Tsai, J.M.; Daneman, M.; Boser, B.E.; Horsley, D.A. Ultrasonic fingerprint sensor using a piezoelectric micromachined ultrasonic transducer array integrated with complementary metal oxide semiconductor electronics. *Appl. Phys. Lett.* **2015**, *106*, 263503. [[CrossRef](#)]
- van Neer, P.L.M.J.; Robers, T.; Volker, A.W.F. A pMUT based flowmeter: A feasibility study. In Proceedings of the 2013 IEEE International Ultrasonics Symposium (IUS), Prague, Czech Republic, 21–25 July 2013; pp. 1319–1322.
- Horsley, D.A.; Przybyla, R.J.; Shelton, S.E.; Goericke, F.T.; Eovino, B.E.; Alex, M.; Logan, J. Piezoelectric Micromachined Ultrasonic Transducers for Range-Finding Applications. In Proceedings of the 2021 5th IEEE Electron Devices Technology & Manufacturing Conference (EDTM), Chengdu, China, 8–11 April 2021; pp. 1–3.
- Robichaud, A.; Cicek, P.-V.; Deslandes, D.; Nabki, F. Frequency Tuning Technique of Piezoelectric Ultrasonic Transducers for Ranging Applications. *J. Microelectromechanical Syst.* **2018**, *27*, 570–579. [[CrossRef](#)]
- Przybyla, R.; Flynn, A.; Jain, V.; Shelton, S.; Guedes, A.; Izumirin, I.; Horsley, D.; Boser, B. A micromechanical ultrasonic distance sensor with >1 meter range. In Proceedings of the 2011 16th International Solid-State Sensors, Actuators and Microsystems Conference, Beijing, China, 5–9 June 2011; pp. 2070–2073.
- Gijsenbergh, P.; Halbach, A.; Jeong, Y.; Torri, G.B.; Billen, M.; Demi, L.; Huang, C.-H.; Cheyns, D.; Rottenberg, X.; Rochus, V. Characterization of polymer-based piezoelectric micromachined ultrasound transducers for short-range gesture recognition applications. *J. Micromech. Microeng.* **2019**, *29*, 074001. [[CrossRef](#)]
- Przybyla, R.J.; Tang, H.-Y.; Guedes, A.; Shelton, S.E.; Horsley, D.A.; Boser, B.E. 3D Ultrasonic Rangefinder on a Chip. *IEEE J. Solid-St. Circ.* **2015**, *50*, 320–334. [[CrossRef](#)]
- Lu, Y. Piezoelectric Micromachined Ultrasonic Transducers for Fingerprint Sensing. Ph.D. Thesis, Mechanical and Aerospace Engineering, University of California, Oakland, CA, USA, 2015.
- Zhou, Z.; Yoshida, S.; Tanaka, S. Epitaxial PMnN-PZT/Si MEMS ultrasonic rangefinder with 2 m range at 1 V drive. *Sens. Actuators A Phys.* **2017**, *266*, 352–360. [[CrossRef](#)]
- Przybyla, R.J.; Tang, H.-Y.; Shelton, S.E.; Horsley, D.A.; Boser, B.E. 12.1 3D ultrasonic gesture recognition. In Proceedings of the 2014 IEEE International Solid-State Circuits Conference Digest of Technical Papers (ISSCC), San Francisco, CA, USA, 9–13 February 2014; pp. 210–211.
- Kanda, T.; Makino, A.; Ono, T.; Suzumori, K.; Morita, T.; Kurosawa, M.K. A micro ultrasonic motor using a micro-machined cylindrical bulk PZT transducer. *Sens. Actuators A Phys.* **2006**, *127*, 131–138. [[CrossRef](#)]
- Wang, T.; Kobayashi, T.; Lee, C. Highly sensitive piezoelectric micromachined ultrasonic transducer operated in air. *Micro Nano Lett.* **2016**, *11*, 558–562. [[CrossRef](#)]
- Qiu, Z.; Lu, Y.; Qiu, Z. Review of Ultrasonic Ranging Methods and Their Current Challenges. *Micromachines* **2022**, *13*, 520. [[CrossRef](#)]
- Toda, M. New type of matching layer for air-coupled ultrasonic transducers. *IEEE Trans. Ultrason. Ferroelectr. Freq. Control* **2002**, *49*, 972–979. [[CrossRef](#)]
- Akasheh, F.; Myers, T.; Fraser, J.D.; Bose, S.; Bandyopadhyay, A. Development of piezoelectric micromachined ultrasonic transducers. *Sens. Actuators A Phys.* **2004**, *111*, 275–287. [[CrossRef](#)]
- Wang, T.; Lee, C. Zero-Bending Piezoelectric Micromachined Ultrasonic Transducer (pMUT) With Enhanced Transmitting Performance. *J. Microelectromechanical Syst.* **2015**, *24*, 2083–2091. [[CrossRef](#)]

23. Yang, Y.; Tian, H.; Wang, Y.F.; Shu, Y.; Zhou, C.J.; Sun, H.; Zhang, C.H.; Chen, H.; Ren, T.L. An ultra-high element density pMUT array with low crosstalk for 3-D medical imaging. *Sensors* **2013**, *13*, 9624–9634. [[CrossRef](#)]
24. Herrera, B.; Pop, F.; Cassella, C.; Rinaldi, M. Miniaturized PMUT-Based Receiver for Underwater Acoustic Networking. *J. Microelectromechanical Syst.* **2020**, *29*, 832–838. [[CrossRef](#)]
25. Pala, S.; Lin, L. Piezoelectric Micromachined Ultrasonic Transducers (pMUT) with Free Boundary. In Proceedings of the 2020 IEEE International Ultrasonics Symposium (IUS), Las Vegas, NV, USA, 7–11 September 2020; pp. 1–4.
26. Dausch, D.E.; Gilchrist, K.H.; Carlson, J.R.; Castellucci, J.B.; Chou, D.R.; von Ramm, O.T. Improved pulse-echo imaging performance for flexure-mode pMUT arrays. In Proceedings of the 2010 IEEE International Ultrasonics Symposium, San Diego, CA, USA, 11–14 October 2010; pp. 451–454.
27. Muralt, P.; Ledermann, N.; Baborowski, J.; Barzegar, A.; Gentil, S.; Belgacem, B.; Petitgrand, S.; Bosseboeuf, A.; Setter, N. Piezoelectric micromachined ultrasonic transducers based on PZT thin films. *IEEE Trans. Ultrason. Ferroelectr. Freq. Control* **2005**, *52*, 2276–2288. [[CrossRef](#)]
28. Liu, W.; He, L.; Wang, X.; Zhou, J.; Xu, W.; Smagin, N.; Toubal, M.; Yu, H.; Gu, Y.; Xu, J.; et al. 3D FEM Analysis of High-Frequency AlN-Based PMUT Arrays on Cavity SOI. *Sensors* **2019**, *19*, 4450. [[CrossRef](#)]
29. Zhao, L.; Annayev, M.; Oralkan, O.; Jia, Y. An Ultrasonic Energy Harvesting IC Providing Adjustable Bias Voltage for Pre-Charged CMUT. *IEEE Trans. Biomed. Circuits Syst.* **2022**, *16*, 842–851. [[CrossRef](#)]
30. Wygant, I.O.; Kupnik, M.; Windsor, J.C.; Wright, W.M.; Wochner, M.S.; Yaralioglu, G.G.; Hamilton, M.F.; Khuri-Yakub, B.T. 50 kHz capacitive micromachined ultrasonic transducers for generation of highly directional sound with parametric arrays. *IEEE Trans. Ultrason. Ferroelectr. Freq. Control* **2009**, *56*, 193–203. [[CrossRef](#)]
31. Yang, H.; Ji, M.; Xiu, X.; Lv, H.; Gu, A.; Zhang, S. AlScN Film Based Piezoelectric Micromechanical Ultrasonic Transducer for an Extended Long-Range Detection. *Micromachines* **2022**, *13*, 1942. [[CrossRef](#)] [[PubMed](#)]
32. Birjis, Y.; Swaminathan, S.; Nazemi, H.; Raj, G.C.A.; Munirathinam, P.; Abu-Libdeh, A.; Emadi, A. Piezoelectric Micromachined Ultrasonic Transducers (PMUTs): Performance Metrics, Advancements, and Applications. *Sensors* **2022**, *22*, 9151. [[CrossRef](#)]
33. Przybyla, R.; Izumkin, I.; Kline, M.; Boser, B.; Shelton, S. An ultrasonic rangefinder based on an AlN piezoelectric micromachined ultrasound transducer. In Proceedings of the 2010 IEEE Sensors, Waikoloa, HI, USA, 1–4 November 2010; pp. 2417–2421.
34. Zhou, Z.; Yoshida, S.; Tanaka, S. Monocrystalline PMNN-PZT thin film ultrasonic rangefinder with 2 meter range at 1 volt drive. In Proceedings of the 2017 19th International Conference on Solid-State Sensors, Actuators and Microsystems (TRANSDUCERS), Kaohsiung, Taiwan, 18–22 June 2017; pp. 167–170.
35. Chen, X.; Xu, J.; Chen, H.; Ding, H.; Xie, J. High-Accuracy Ultrasonic Rangefinders via pMUTs Arrays Using Multi-Frequency Continuous Waves. *J. Microelectromechanical Syst.* **2019**, *28*, 634–642. [[CrossRef](#)]
36. Alasatri, S.; Rufer, L.; Lee, J.E.-Y. AlN-on-Si Square Diaphragm Piezoelectric Micromachined Ultrasonic Transducer with Extended Range of Detection. In Proceedings of the Eurosensors 2018, Graz, Austria, 9–12 September 2018.
37. Skolnik, M. *Introduction to Radar Systems*, 3rd ed.; McGraw-Hill: New York, NY, USA, 2001.
38. Parrilla, M.; Anaya, J.J.; Fritsch, C. Digital signal processing techniques for high accuracy ultrasonic range measurements. *IEEE Trans. Instrum. Meas.* **1991**, *40*, 759–763. [[CrossRef](#)]
39. Suresh, A.; Mak, K.L.; Benserhir, J.; Lee, J.E.Y.; Rufer, L. Air-coupled Ultrasonic Rangefinder with Meter-long Detection Range Based on a Dual-electrode PMUT Fabricated Using a Multi-user MEMS Process. In Proceedings of the 2019 IEEE Sensors, Montreal, QC, Canada, 27–30 October 2019; pp. 1–4.
40. Blackstock, D.T. *Fundamentals of Physical Acoustics*; John Wiley and Sons: Hoboken, NJ, USA, 2000.
41. Ledesma, E.; Zamora, I.; Uranga, A.; Barniol, N. Tent-Plate AlN PMUT With a Piston-Like Shape Under Liquid Operation. *IEEE Sens. J.* **2020**, *20*, 11128–11137. [[CrossRef](#)]
42. Ledesma, E.; Zamora, I.; Torres, F.; Uranga, A.; Tzanov, V.; Barniol, N.; Marigó, E.; Soundara-Pandian, M. Squared PMUT with Enhanced Pressure Sensitivities. In Proceedings of the Eurosensors 2018, Graz, Austria, 9–12 September 2018.
43. Kinsler, L.E.; Frey, A.R.; Coppens, A.B.; Sanders, J.V. *Fundamentals of Acoustics*, 4th ed.; Wiley Publications: Hoboken, NJ, USA, 2000.
44. Wang, H.; Ma, Y.; Yang, H.; Jiang, H.; Ding, Y.; Xie, H. MEMS Ultrasound Transducers for Endoscopic Photoacoustic Imaging Applications. *Micromachines* **2020**, *11*, 928. [[CrossRef](#)]
45. Kuratli, C.; Qiuting, H. A CMOS ultrasound range-finder microsystem. *IEEE J. Solid-St. Circ.* **2000**, *35*, 2005–2017. [[CrossRef](#)]
46. Zamora, I.; Ledesma, E.; Uranga, A.; Barniol, N. High Accuracy Ultrasound Micro-Distance Measurements with PMUTs under Liquid Operation. *Sensors* **2021**, *21*, 4524. [[CrossRef](#)] [[PubMed](#)]
47. Webster, D. A pulsed ultrasonic distance measurement system based upon phase digitizing. *IEEE Trans. Instrum. Meas.* **1994**, *43*, 578–582. [[CrossRef](#)]
48. Green, E.I. The story of Q. *Am. Sci.* **1955**, *43*, 584–594.
49. Jeong, J.J.; Choi, H. An impedance measurement system for piezoelectric array element transducers. *Measurement* **2017**, *97*, 138–144. [[CrossRef](#)]
50. Rozen, O.; Block, S.T.; Shelton, S.E.; Horsley, D.A. Piezoelectric micromachined ultrasonic transducer with increased output pressure via concentric venting rings. In Proceedings of the 2015 Transducers-2015 18th International Conference on Solid-State Sensors, Actuators and Microsystems (TRANSDUCERS), Anchorage, AK, USA, 21–25 June 2015; pp. 670–673.

51. Nayak, B.; Gupta, H.; Roy, K.; Ashok, A.; Shastri, V.; Pratap, R. An Experimental Study of the Acoustic Field of a Single-Cell Piezoelectric Micromachined Ultrasound Transducer (PMUT). In Proceedings of the 2020 5th IEEE International Conference on Emerging Electronics (ICEE), New Delhi, India, 26–28 November 2020; pp. 1–4.
52. Przybyla, R.J.; Shelton, S.E.; Guedes, A.; Krigel, R.; Horsley, D.A.; Boser, B.E. In-Air Rangefinding and Angle Estimation Using an Array of AlN Micromachined Transducers. In Proceedings of the 2012 Solid-State, Actuators, and Microsystems Workshop Technical Digest, Hilton Head, SC, USA, 3–7 June 2012; pp. 50–53.
53. Wang, M.; Zhou, Y. Design of piezoelectric micromachined ultrasonic transducers (pMUTs) for high pressure output. *Microsyst. Technol.* **2016**, *23*, 1761–1766. [[CrossRef](#)]
54. Dangi, A.; Pratap, R. System level modeling and design maps of PMUTs with residual stresses. *Sens. Actuators A Phys.* **2017**, *262*, 18–28. [[CrossRef](#)]
55. Rozen, O.; Block, S.T.; Mo, X.; Bland, W.; Hurst, P.; Tsai, J.M.; Daneman, M.; Amirtharajah, R.; Horsley, D.A. Monolithic MEMS-CMOS ultrasonic rangefinder based on dual-electrode PMUTs. In Proceedings of the 2016 IEEE 29th International Conference on Micro Electro Mechanical Systems (MEMS), Shanghai, China, 24–28 January 2016; pp. 115–118.
56. Herrera, B.; Pop, F.; Cassella, C.; Rinaldi, M. AlN PMUT-based Ultrasonic Power Transfer Links for Implantable Electronics. In Proceedings of the 2019 20th International Conference on Solid-State Sensors, Actuators and Microsystems & Eurosensors XXXIII (TRANSDUCERS & EUROSENSORS XXXIII), Berlin, Germany, 23–27 June 2019; pp. 861–864.
57. Chen, M.; Zhang, Q.; Zhao, X.; Wang, F.; Liu, H.; Li, B.; Zhang, X.; Luo, H. Design and analysis of piezoelectric micromachined ultrasonic transducer using high coupling PMN-PT single crystal thin film for ultrasound imaging. *Smart Mater. Struct.* **2021**, *30*, 055006. [[CrossRef](#)]
58. Li, B.; Sun, C.; Xin, S.; Luo, M.; Hei, C.; Du, G.; Feng, A. Development of a 16-Channel Broadband Piezoelectric Micro Ultrasonic Transducer Array Probe for Pipeline Butt-Welded Defect Detection. *Sensors* **2022**, *22*, 7133. [[CrossRef](#)]
59. Liao, W.; Liu, W.; Rogers, J.E.; Usmani, F.; Tang, Y.; Wang, B.; Jiang, H.; Xie, H. Piezoelectric micromachined ultrasound transducer array for photoacoustic imaging. In Proceedings of the 2013 Transducers & Eurosensors XXVII: The 17th International Conference on Solid-State Sensors, Actuators and Microsystems (TRANSDUCERS & EUROSENSORS XXVII), Barcelona, Spain, 16–20 June 2013; pp. 1831–1834.
60. Cai, J.; Liu, K.; Lou, L.; Zhang, S.; Gu, Y.A.; Wu, T. Increasing Ranging Accuracy of Aluminum Nitride Pmuts by Circuit Coupling. In Proceedings of the 2021 IEEE 34th International Conference on Micro Electro Mechanical Systems (MEMS), Gainesville, FL, USA, 25–29 January 2021; pp. 740–743.
61. Wang, T.; Kobayashi, T.; Yang, B.; Wang, H.; Lee, C. Highly sensitive piezoelectric micromachined ultrasonic transducer (pMUT) operated in air. In Proceedings of the 2016 IEEE 11th Annual International Conference on Nano/Micro Engineered and Molecular Systems (NEMS), Sendai, Japan, 17–20 April 2016; pp. 294–299.
62. Cai, G.; Zhou, X.; Yi, Y.; Zhou, H.; Li, D.; Zhang, J.; Huang, H.; Mu, X. An Enhanced-Differential PMUT for Ultra-Long Distance Measurement in Air. In Proceedings of the 2021 IEEE 34th International Conference on Micro Electro Mechanical Systems (MEMS), Gainesville, FL, USA, 25–29 January 2021; pp. 899–902.
63. Kusano, Y.; Luo, G.-L.; Horsley, D.A. Spurious Mode Free Hexagonal PMUT Array. In Proceedings of the 2019 20th International Conference on Solid-State Sensors, Actuators and Microsystems & Eurosensors XXXIII (TRANSDUCERS & EUROSENSORS XXXIII), Berlin, Germany, 23–27 June 2019; pp. 238–241.
64. Sun, S.; Wang, J.; Zhang, M.; Yuan, Y.; Ning, Y.; Ma, D.; Niu, P.; Gong, Y.; Yang, X.; Pang, W. Eye-Tracking Monitoring Based on PMUT Arrays. *J. Microelectromechanical Syst.* **2022**, *31*, 45–53. [[CrossRef](#)]
65. Jung, J.; Kim, S.; Lee, W.; Choi, H. Fabrication of a two-dimensional piezoelectric micromachined ultrasonic transducer array using a top-crossover-to-bottom structure and metal bridge connections. *J. Micromech. Microeng.* **2013**, *23*, 125037. [[CrossRef](#)]
66. Jung, J.; Lee, W.; Kang, W.; Hong, H.; Song, H.Y.; Oh, I.-y.; Park, C.S.; Choi, H. A top-crossover-to-bottom addressed segmented annular array using piezoelectric micromachined ultrasonic transducers. *J. Micromech. Microeng.* **2015**, *25*, 115024. [[CrossRef](#)]
67. Xu, T.; Zhao, L.; Jiang, Z.; Guo, S.; Li, Z.; Yang, P.; Sun, L.; Luo, G.; Zhang, L. Array Design of Piezoelectric Micromachined Ultrasonic Transducers With Low-Crosstalk and High-Emission Performance. *IEEE Trans. Ultrason. Ferroelectr. Freq. Control* **2020**, *67*, 789–800. [[CrossRef](#)] [[PubMed](#)]
68. Vysotskyi, B.; Haouari, R.; Weekers, B.; Keulemans, G.; Torri, G.B.; Rochus, V. A comparative study of acoustic isolation configurations for pMUT array-based applications. In Proceedings of the 2021 22nd International Conference on Thermal, Mechanical and Multi-Physics Simulation and Experiments in Microelectronics and Microsystems (EuroSimE), St. Julian, Malta, 19–21 April 2021; pp. 1–5.
69. Przybyla, R.J.; Shelton, S.E.; Guedes, A.; Izumirin, I.I.; Kline, M.H.; Horsley, D.A.; Boser, B.E. In-Air Rangefinding With an AlN Piezoelectric Micromachined Ultrasound Transducer. *IEEE Sens. J.* **2011**, *11*, 2690–2697. [[CrossRef](#)]
70. Luo, G.-L.; Kusano, Y.; Horsley, D.A. Airborne Piezoelectric Micromachined Ultrasonic Transducers for Long-Range Detection. *J. Microelectromechanical Syst.* **2021**, *30*, 81–89. [[CrossRef](#)]
71. Liu, X.; Chen, X.; Le, X.; Xu, Z.; Wu, C.; Xie, J. A High-Performance Square pMUT for Range-finder. In Proceedings of the 2018 IEEE 13th Annual International Conference on Nano/Micro Engineered and Molecular Systems (NEMS), Singapore, 22–26 April 2018; pp. 106–109.
72. Chiu, Y.; Wang, C.; Gong, D.; Li, N.; Ma, S.; Jin, Y. A Novel Ultrasonic TOF Ranging System Using AlN Based PMUTs. *Micromachines* **2021**, *12*, 284. [[CrossRef](#)]

73. Akhbari, S.; Sammoura, F.; Eovino, B.; Yang, C.; Lin, L. Bimorph Piezoelectric Micromachined Ultrasonic Transducers. *J. Microelectromechanical Syst.* **2016**, *25*, 326–336. [[CrossRef](#)]
74. Akhbari, S.; Sammoura, F.; Yang, C.; Mahmoud, M.; Aqab, N.; Lin, L. Bimorph pMUT with dual electrodes. In Proceedings of the 2015 28th IEEE International Conference on Micro Electro Mechanical Systems (MEMS), Estoril, Portugal, 18–22 January 2015; pp. 928–931.
75. Shao, Z.; Pala, S.; Peng, Y.; Lin, L. Bimorph Pinned Piezoelectric Micromachined Ultrasonic Transducers for Space Imaging Applications. *J. Microelectromechanical Syst.* **2021**, *30*, 650–658. [[CrossRef](#)]
76. Shao, Z.; Peng, Y.; Pala, S.; Liang, Y.; Lin, L. 3D Ultrasonic Object Detections with >1 Meter Range. In Proceedings of the 2021 IEEE 34th International Conference on Micro Electro Mechanical Systems (MEMS), Gainesville, FL, USA, 25–29 January 2021; pp. 386–389.
77. Nistorica, C.; Latev, D.; Mendoza, J.; Imai, D. Modeling and characterization of a 3D-MEMS piezoelectric ultrasound transducer. In Proceedings of the 2016 IEEE International Ultrasonics Symposium (IUS), Tours, France, 18–21 September 2016; pp. 1–4.
78. Stoppel, F.; Mannchen, A.; Niekiel, F.; Beer, D.; Giese, T.; Wagner, B. New integrated full-range MEMS speaker for in-ear applications. In Proceedings of the 2018 IEEE Micro Electro Mechanical Systems (MEMS), Belfast, UK, 21–25 January 2018; pp. 1068–1071.
79. Jung, J.; Lee, W.; Kang, W.; Shin, E.; Ryu, J.; Choi, H. Review of piezoelectric micromachined ultrasonic transducers and their applications. *J. Micromech. Microeng.* **2017**, *27*, 113001. [[CrossRef](#)]
80. Yoshida, S.; Hanzawa, H.; Wasa, K.; Tanaka, S. Fabrication and characterization of large figure-of-merit epitaxial PMnN-PZT/Si transducer for piezoelectric MEMS sensors. *Sens. Actuators A Phys.* **2016**, *239*, 201–208. [[CrossRef](#)]
81. Luo, G.-L.; Kusano, Y.; Roberto, M.N.; Horsley, D.A. High-Pressure Output 40 kHz Air-Coupled Piezoelectric Micromachined Ultrasonic Transducers. In Proceedings of the 2019 IEEE 32nd International Conference on Micro Electro Mechanical Systems (MEMS), Seoul, Republic of Korea, 27–31 January 2019; pp. 787–790.
82. Cheng, C.; Peters, T.; Dangi, A.; Agrawal, S.; Chen, H.; Kothapalli, S.R.; Trolier-McKinstry, S. Improving PMUT Receive Sensitivity via DC Bias and Piezoelectric Composition. *Sensors* **2022**, *22*, 5614. [[CrossRef](#)]
83. Ngoc Thao, P.; Yoshida, S.; Tanaka, S. Fabrication and Characterization of PZT Fibered-Epitaxial Thin Film on Si for Piezoelectric Micromachined Ultrasound Transducer. *Micromachines* **2018**, *9*, 455. [[CrossRef](#)] [[PubMed](#)]
84. Li, J.; Ren, W.; Fan, G.; Wang, C. Design and Fabrication of Piezoelectric Micromachined Ultrasound Transducer (pMUT) with Partially-Etched ZnO Film. *Sensors* **2017**, *17*, 1381. [[CrossRef](#)]
85. Sadeghpour, S.; Puers, R. Optimization in the Design and Fabrication of a PZT Piezoelectric Micromachined Ultrasound Transducer (PMUT). In Proceedings of the Eurosensors 2018, Graz, Austria, 9–12 September 2018.
86. Yu, Q.; Fan, G.; Ren, W.; Fan, Q.; Ti, J.; Li, J.; Wang, C. PZT-Film-Based Piezoelectric Micromachined Ultrasonic Transducer with I-Shaped Composite Diaphragm. *Micromachines* **2022**, *13*, 1597. [[CrossRef](#)] [[PubMed](#)]
87. Wang, H.; Yu, Y.; Chen, Z.; Yang, H.; Jiang, H.; Xie, H. Design and Fabrication of a Piezoelectric Micromachined Ultrasonic Transducer Array Based on Ceramic PZT. In Proceedings of the 2018 IEEE Sensors, New Delhi, India, 28–31 October 2018; pp. 1–4.
88. Cai, J.; Wang, Y.; Lou, L.; Zhang, S.; Gu, Y.; Gao, F.; Wu, T. Photoacoustic and Ultrasound Dual-Modality Endoscopic Imaging Based on ALN Pmut Array. In Proceedings of the 2022 IEEE 35th International Conference on Micro Electro Mechanical Systems Conference (MEMS), Tokyo, Japan, 9–13 January 2022; pp. 412–415.
89. Zang, J.; Fan, Z.; Li, P.; Duan, X.; Wu, C.; Cui, D.; Xue, C. Design and Fabrication of High-Frequency Piezoelectric Micromachined Ultrasonic Transducer Based on an ALN Thin Film. *Micromachines* **2022**, *13*, 1317. [[CrossRef](#)] [[PubMed](#)]
90. Cai, J.; Wang, Y.; Jiang, D.; Zhang, S.; Gu, Y.A.; Lou, L.; Gao, F.; Wu, T. Beyond fundamental resonance mode: High-order multi-band ALN PMUT for in vivo photoacoustic imaging. *Microsyst. Nanoeng.* **2022**, *8*, 116. [[CrossRef](#)] [[PubMed](#)]
91. Shelton, S.; Chan, M.-L.; Park, H.; Horsley, D.; Boser, B.; Izuyumin, I.; Przybyla, R.; Frey, T.; Judy, M.; Nunan, K.; et al. CMOS-compatible AlN piezoelectric micromachined ultrasonic transducers. In Proceedings of the 2009 IEEE International Ultrasonics Symposium, Rome, Italy, 20–23 September 2009; pp. 402–405.
92. Trolier-McKinstry, S.; Muralt, P. Thin Film Piezoelectrics for MEMS. *J. Electroceramics* **2004**, *12*, 7–17. [[CrossRef](#)]
93. Chen, B.; Chu, F.; Liu, X.; Li, Y.; Rong, J.; Jiang, H. AlN-based piezoelectric micromachined ultrasonic transducer for photoacoustic imaging. *Appl. Phys. Lett.* **2013**, *103*, 031118. [[CrossRef](#)]
94. Yipeng, L.; Hao-Yen, T.; Fung, S.; Boser, B.E.; Horsley, D.A. Short-range and high-resolution ultrasound imaging using an 8 MHz aluminum nitride PMUT array. In Proceedings of the 2015 28th IEEE International Conference on Micro Electro Mechanical Systems (MEMS), Estoril, Portugal, 18–22 January 2015; pp. 140–143.
95. Wasa, K.; Matsushima, T.; Adachi, H.; Kanno, I.; Kotera, H. Thin-Film Piezoelectric Materials For a Better Energy Harvesting MEMS. *J. Microelectromechanical Syst.* **2012**, *21*, 451–457. [[CrossRef](#)]
96. Luo, G.-L.; Kusano, Y.; Horsley, D. Immersion PMUTs Fabricated with a Low Thermal-Budget Surface Micromachining Process. In Proceedings of the 2018 IEEE International Ultrasonics Symposium (IUS), Kobe, Japan, 22–25 October 2018; pp. 1–4.
97. Horsley, D.; Lu, Y.; Rozen, O. Flexural Piezoelectric Resonators. In *Piezoelectric MEMS Resonators*; Bhugra, H., Piazza, G., Eds.; Springer International Publishing: Cham, Switzerland, 2017; pp. 153–173.
98. Muralt, P. Which is the best thin film piezoelectric material? In Proceedings of the 2017 IEEE International Ultrasonics Symposium (IUS), Washington, DC, USA, 6–9 September 2017; pp. 1–3.

99. Wang, Q.; Lu, Y.; Mishin, S.; Oshmyansky, Y.; Horsley, D.A. Design, Fabrication, and Characterization of Scandium Aluminum Nitride-Based Piezoelectric Micromachined Ultrasonic Transducers. *J. Microelectromechanical Syst.* **2017**, *26*, 1132–1139. [[CrossRef](#)]
100. Akiyama, M.; Umeda, K.; Honda, A.; Nagase, T. Influence of scandium concentration on power generation figure of merit of scandium aluminum nitride thin films. *Appl. Phys. Lett.* **2013**, *102*, 021915. [[CrossRef](#)]
101. Kusano, Y.; Ishii, I.; Kamiya, T.; Teshigahara, A.; Luo, G.L.; Horsley, D.A. High-SPL Air-Coupled Piezoelectric Micromachined Ultrasonic Transducers Based on 36% ScAlN Thin-Film. *IEEE Trans. Ultrason. Ferroelectr. Freq. Control* **2019**, *66*, 1488–1496. [[CrossRef](#)]
102. Feng, G.H.; Liu, H.J. Piezoelectric Micromachined Ultrasonic Transducers with a Cost-Effective Bottom-Up Fabrication Scheme for Millimeter-Scale Range Finding. *Sensors* **2019**, *19*, 4696. [[CrossRef](#)] [[PubMed](#)]
103. Haynes, W.M. *CRC Handbook of Chemistry and Physics*, 95th ed.; CRC Press: Boca Raton, FL, USA, 2014. [[CrossRef](#)]
104. Marioli, D.; Narduzzi, C.; Offelli, C.; Petri, D.; Sardini, E.; Taroni, A. Digital time-of-flight measurement for ultrasonic sensors. *IEEE Trans. Instrum. Meas.* **1992**, *41*, 93–97. [[CrossRef](#)]
105. Carotenuto, R.; Merenda, M.; Iero, D.; G. Della Corte, F. Simulating Signal Aberration and Ranging Error for Ultrasonic Indoor Positioning. *Sensors* **2020**, *20*, 3548. [[CrossRef](#)] [[PubMed](#)]
106. Koh, Y.; Wai Choong, D.S.; Chen, D.S.-H.; Goh, D.J.; Ghosh, S.; Sharma, J.; Merugu, S.; Quaglia, F.; Ferrera, M.; Savoia, A.S.; et al. High Resolution, High Frequency Ultrasonic Ranging in Air with pMUTs. In Proceedings of the 2021 IEEE International Ultrasonics Symposium (IUS), Xi'an, China, 11–16 September 2021; pp. 1–4.
107. Wu, Z.; Liu, W.; Tong, Z.; Zhang, S.; Gu, Y.; Wu, G.; Tovstopyat, A.; Sun, C.; Lou, L. A Novel Transfer Function Based Ring-Down Suppression System for PMUTs. *Sensors* **2021**, *21*, 6414. [[CrossRef](#)]
108. Pala, S.; Shao, Z.; Peng, Y.; Lin, L. Improved Ring-Down Time and Axial Resolution of pMUTs via a Phase-Shift Excitation Scheme. In Proceedings of the 2021 IEEE 34th International Conference on Micro Electro Mechanical Systems (MEMS), Gainesville, FL, USA, 25–29 January 2021; pp. 390–393.
109. Huang, Y.P.; Wang, J.S.; Huang, K.N.; Ho, C.T.; Huang, J.D.; Young, M.S. Envelope pulsed ultrasonic distance measurement system based upon amplitude modulation and phase modulation. *Rev. Sci. Instrum.* **2007**, *78*, 065103. [[CrossRef](#)] [[PubMed](#)]
110. Hong, H.; Yongtian, W.; Dayuan, Y. A low-cost dynamic range-finding device based on amplitude-modulated continuous ultrasonic wave. *IEEE Trans. Instrum. Meas.* **2002**, *51*, 362–367. [[CrossRef](#)]
111. Huang, C.F.; Young, M.S.; Li, Y.C. Multiple-frequency continuous wave ultrasonic system for accurate distance measurement. *Rev. Sci. Instrum.* **1999**, *70*, 1452–1458. [[CrossRef](#)]
112. Chongchamsai, M.; Sinchai, S.; Wardkein, P.; Boonjun, S. Distance Measurement Technique Using Phase Difference of Two Reflected Ultrasonic Frequencies. In Proceedings of the 2018 3rd International Conference on Computer and Communication Systems (ICCCS), Nagoya, Japan, 27–30 April 2018; pp. 372–376.
113. Dostart, N.; Brand, M.; Zhang, B.; Feldkhun, D.; Wagner, K.; Popović, M.A. Vernier Si-Photonic Phased Array Transceiver for Grating Lobe Suppression and Extended Field-of-View. In Proceedings of the Conference on Lasers and Electro-Optics, San Jose, CA, USA, 5–10 May 2019.
114. Demi, L. Practical Guide to Ultrasound Beam Forming: Beam Pattern and Image Reconstruction Analysis. *Appl. Sci.* **2018**, *8*, 1544. [[CrossRef](#)]
115. Fain, B.; Blard, F.; Bastien, J.-C.; Gardien, F.; Frassati, F. Beamforming with AlN-based bimorph piezoelectric micromachined ultrasonic transducers. In Proceedings of the 2021 Smart Systems Integration (SSI), Grenoble, France, 27–29 April 2021; pp. 1–4.

Disclaimer/Publisher’s Note: The statements, opinions and data contained in all publications are solely those of the individual author(s) and contributor(s) and not of MDPI and/or the editor(s). MDPI and/or the editor(s) disclaim responsibility for any injury to people or property resulting from any ideas, methods, instructions or products referred to in the content.